

# Effect of DNA interaction involving antioxidative 4-aminoantipyrine incorporating mixed ligand complexes having alpha-amino acid as co-ligand



Natarajan Raman<sup>a,\*</sup>, Arunagiri Sakthivel<sup>a</sup>, Muthusamy Selvaganapathy<sup>a</sup>, Liviu Mitu<sup>b</sup>

<sup>a</sup> Research Department of Chemistry, VHNSN College, Virudhunagar 626 001, India

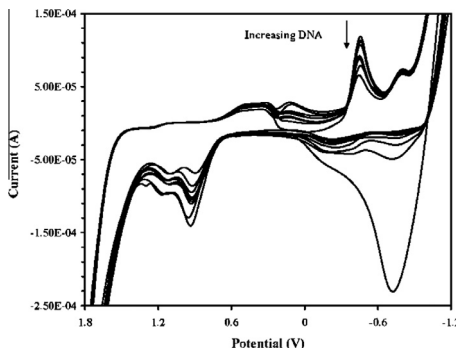
<sup>b</sup> Department of Chemistry, University of Pitesti, Pitesti 110040, Romania

## HIGHLIGHTS

- Exploring efficient antioxidative agents having amino acid as co-ligand.
- Excellent  $K_b$  values for valine mixed ligand complexes.
- Effective cleavage of pUC19 DNA via oxidative pathway.
- Better antimicrobial active agents.

## GRAPHICAL ABSTRACT

Few novel 4-aminoantipyrine incorporating amino acid mixed ligand complexes act as efficient DNA binding and DNA cleaving agents due to the size of the alkyl group present in the amino acid. They are good antimicrobial and oxidative activators.



## ARTICLE INFO

### Article history:

Received 28 October 2013

Received in revised form 6 December 2013

Accepted 16 December 2013

Available online 21 December 2013

### Keywords:

Binding constant

4-Aminoantipyrine

pUC19 DNA

Minimum inhibitory concentration (MIC)

Antioxidant

## ABSTRACT

Few new mixed ligand transition metal complexes of the stoichiometry  $[ML(A)_2]$ , where  $M = Co(II), Ni(II), Cu(II)$  and  $Zn(II)$ ,  $L = FFAP$  (furfurylidene-4-aminoantipyrine) and  $A =$  amino acid (glycine/alanine/valine), have been designed, synthesized and characterized. The molar conductivity of the complexes in DMF at  $10^{-3}$  M concentration shows that they are non-electrolytes. The interaction of these complexes with CT-DNA indicates that the valine mixed ligand complexes are having higher binding constant than alanine and glycine mixed ligand complexes. This analysis reveals that binding constant depends on the size of the alkyl group present in the amino acid. The binding constants of valine mixed ligand complexes are in the order of  $10^4$  to  $10^5$   $M^{-1}$  revealing that the complexes interact with DNA through moderate intercalation mode. The metal complexes exhibit effective cleavage of pUC19 DNA but it is not preceded via radical cleavage and superoxide anion radical. They are good antimicrobial agents than the free ligand. On comparing the  $IC_{50}$  values,  $[Ni(L)(Gly)_2]$  is considered as a potential drug to eliminate the hydroxyl radical.

© 2013 Elsevier B.V. All rights reserved.

## 1. Introduction

In recent years transition metal complexes have been used widely by many bioinorganic chemists for developing active

transition metal anticancer complexes with better efficiency [1–4]. The interaction of transition metal complexes with DNA has been a subject of passionate research in the field of bioinorganic chemistry, ever since the discovery of cis-platin as an anticancer agent. As an important intention of anticancer drugs, DNA plays a central role in replication, transcription, and regulation of genes. DNA has strong affinity towards many organic compounds and transition

\* Corresponding author. Tel.: +91 9245165958; fax: +91 4562281338.

E-mail address: [drn\\_raman@yahoo.co.in](mailto:drn_raman@yahoo.co.in) (N. Raman).

metal complexes. In its polyionic form, DNA can attract any cationic species and also neutral organic compounds. These compounds may react with or bind to DNA with high affinity and cause the decay of cell at an appropriate time [5].

The presence of metal binding sites in DNA structure make different type of interactions possible such as intercalation between base pairs, minor groove binding, and major groove binding which play an important role in the efforts of the drug targeted to DNA [6,7]. A large number of transition metal complexes have been used as cleavage agents for DNA and also for novel potential DNA-targeted antitumor drugs [8–10]. Additionally, it has been demonstrated that free radicals can damage proteins, lipids, and DNA of bio-tissues, leading to increased rates of cancer [11]. Fortunately, antioxidants can prevent this damage, due to their free radical scavenging activity [12]. Hence, it is very important to develop compounds with both strong antioxidant and DNA-binding properties for effective cancer therapy.

This inspires synthetic chemists to search for new metal complexes for bioactive compounds. Transition metals are particularly suitable for this purpose because they can adopt a wide variety of coordination numbers, geometries and oxidation state in comparison with carbon and other main group elements. It was reported that, the treatment with the copper complexes produce remarkable pharmacological effects, which are not observed when the parent ligands or inorganic forms of copper are used [13]. From a coordination chemistry viewpoint, the only atoms available for coordination are the nitrogen atoms of the pyrazole ring and the oxygen atom of the carbonyl group. If the nitrogens are blocked by substitution, such as in antipyrine, coordination can only be achieved through the oxygen atom. Nowadays, 4-aminoantipyrine derived transition metal complexes have been extensively used in various fields like biological, analytical and therapeutic applications [14]. It has been observed that mixed ligand complexes behave as an efficient DNA-targeted material. The incorporation of an organic compound like  $\alpha$ -amino acid significantly modifies the structural and biological activities of transition metal complexes [15]. In addition to this, the complexes containing 4-aminoantipyrine Schiff base derivative along with  $\alpha$ -amino acids are yet to be explored.

This prompted us to synthesize a new series of heterocyclic compounds containing the antipyrinyl moiety from the Schiff bases derived from furfurylidene-4-aminoantipyrine and  $\alpha$ -amino acids with Co(II), Cu(II), Ni(II) and Zn(II) metal ions. The amino acids are known to coordinate with metal ion through N, O-donor ligand forming five membered chelate ring after dissociation of the acidic proton [16,17]. They are characterized using analytical and spectral techniques. Furthermore, their biological studies like DNA binding, cleavage, antimicrobial, antioxidative responses have been performed.

## 2. Experimental protocols

### 2.1. Reagents and instruments

All reagents, 4-aminoantipyrine, furfural, glycine, alanine, valine and metal(II) chlorides were of Merck products and they were used as supplied. Commercial solvents were distilled and then used for the preparation of ligands and their complexes. DNA was purchased from Bangalore Genei (India). Microanalyses (C, H and N) were performed in Carlo Erba 1108 analyzer at Sophisticated Analytical Instrument Facility (SAIF), Central Drug Research Institute (CDRI), Lucknow, India. Molar conductivities in DMF ( $10^{-3}$  M) at room temperature were measured by using Systronic model-304 digital conductivity meter. Magnetic susceptibility measurement of the complexes was carried out by Gouy balance

using copper sulphate pentahydrate as the calibrant. Infrared spectra ( $4000\text{--}350\text{ cm}^{-1}$  KBr disc) of the samples were recorded on an IR Affinity-1 FT-IR Shimadzu spectrophotometer. NMR spectra were recorded on a Bruker Avance Dry 300 FT-NMR spectrometer in DMSO- $d_6$ , using TMS as the internal reference. Mass spectrometry experiments were performed on a JEOL-AccuTOF JMS-T100LC mass spectrometer equipped with a custom-made electrospray interface (ESI). EPR spectra were recorded on a Varian E 112 EPR spectrometer in DMSO solution both at room temperature (300 K) and liquid nitrogen temperature (77 K) using TCNE (tetracyanoethylene) as the g-marker. The absorption spectra were recorded by using Shimadzu model UV-1601 spectrophotometer at room temperature.

### 2.2. Synthesis of Schiff base (L)

An ethanolic solution of (30 mL) 4-aminoantipyrine (0.01 mol) was added to an ethanolic solution of furfural (0.01 mol). The resultant mixture was refluxed for 3 h. The resulting solution was evaporated under vacuum to remove the solvent. The product was filtered and the yellow coloured solid was isolated and recrystallized in ethanol before drying over desiccators.

L. Yield: 86%. Anal. Calc. for  $C_{16}H_{15}N_3O_2$ : C, 68.4; H, 5.3; N, 14.9 (%); Found: C, 68.3; H, 5.3; N, 14.9 (%). IR (KBr pellet,  $\text{cm}^{-1}$ ): 1665  $\nu(\text{C}=\text{O})$ ; 1645  $\nu(-\text{HC}=\text{N})$ ;  $^1\text{H}$  NMR ( $\delta$ ): (aromatic) 6.6–7.4 (m); (COOH) 11(s); (C–CH<sub>3</sub>) 2.3 (s); (N–CH<sub>3</sub>) 3.1(s); (CH=N) 9.3(s). MS  $m/z$  (%): 282  $[\text{M}+1]^+$ .  $\lambda_{\text{max}}$  ( $\text{cm}^{-1}$ ) in DMF, 35,211, 27,778.

### 2.3. Synthesis of metal complexes

The metal(II) complexes were prepared by mixing the appropriate molar quantity of ligands and metal salt using the following procedure. An ethanolic solution of L (10 mM) was heated under reflux with the ethanolic solution of metal(II) chloride (10 mM) for 3 h. To the above mixture, amino acid (glycine/alanine/valine) (20 mM) in alcoholic potash was added and the reflux was continued for 1 h. The solid product formed was filtered, washed repeatedly with de-ionized water and dried over anhydrous  $\text{CaCl}_2$  under vacuum. Schematic diagram for the synthesis of ligand and metal complexes is given in Scheme 1.

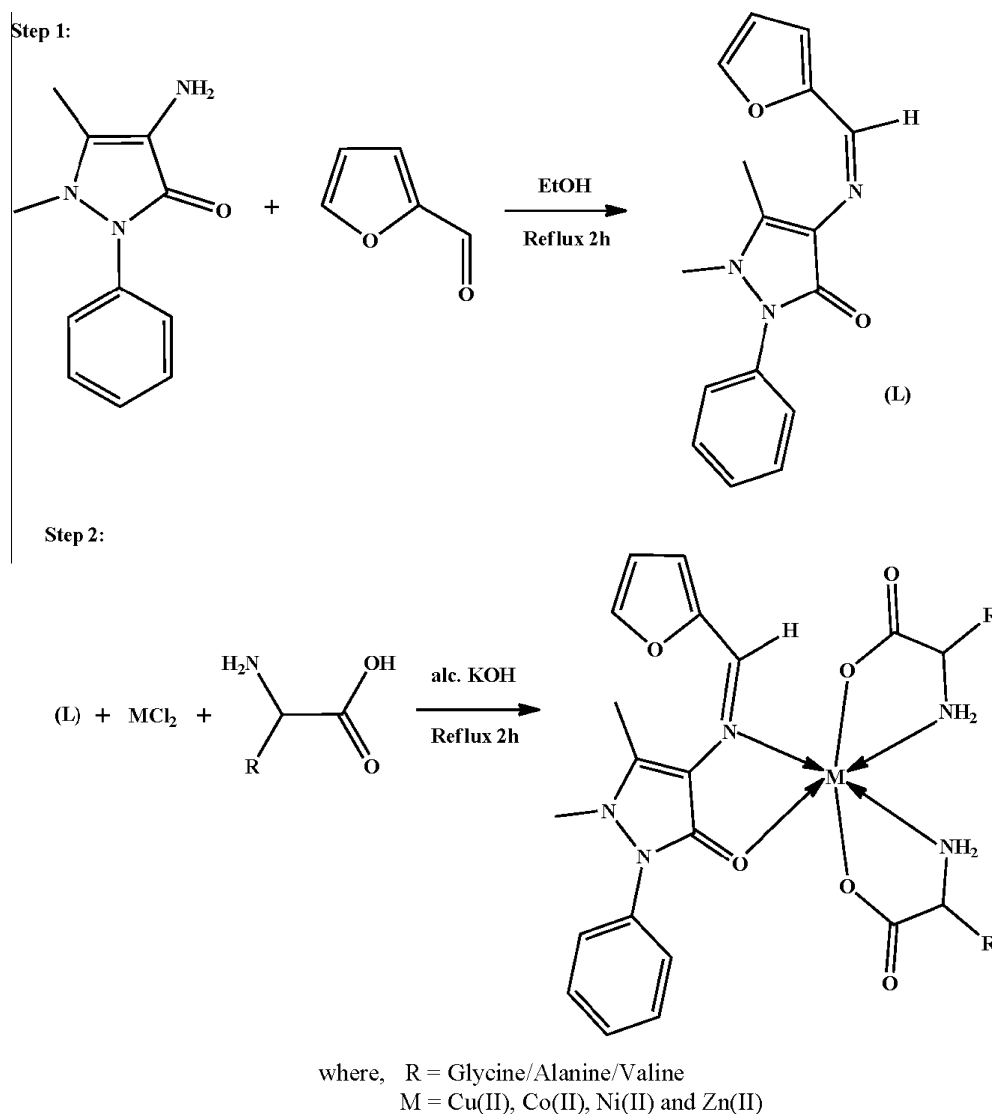
$[\text{Cu}(\text{L})(\text{Gly})_2]$ . Yield: 76%. Anal. Calc. for  $C_{20}H_{23}N_5O_6\text{Cu}$ : Cu, 12.9; C, 48.7; H, 4.7; N, 14.2 (%); Found: Cu, 12.5; C, 48.3; H, 4.2; N, 13.8 (%). IR (KBr pellet,  $\text{cm}^{-1}$ ): 1645  $\nu(\text{C}=\text{O})$ ; 1597  $\nu(-\text{HC}=\text{N})$ ; 3310  $\nu(\text{NH}_2)$ ; 3396, 1406, 1370  $\nu(-\text{COO}^-)$ , ( $-\text{COO}^-$ )  $\nu_{\text{asy}}$ , ( $-\text{COO}^-$ )  $\nu_{\text{sy}}$ ; 503  $\nu(\text{M}-\text{O})$ ; 450  $\nu(\text{M}-\text{N})$ . MS  $m/z$  (%): 493  $[\text{M}+1]^+$ .  $\lambda_{\text{max}}$  ( $\text{cm}^{-1}$ ) in DMF, 11,001, 35,842.  $\mu_{\text{eff}}$  (BM): 1.87.

$[\text{Cu}(\text{L})(\text{Ala})_2]$ . Yield: 72%. Anal. Calc. for  $C_{22}H_{27}N_5O_6\text{Cu}$ : Cu, 12.2; C, 50.7; H, 5.2; N, 13.4 (%); Found: Cu, 11.7; C, 50.2; H, 4.8; N, 13.1 (%). IR (KBr pellet,  $\text{cm}^{-1}$ ): 1643  $\nu(\text{C}=\text{O})$ ; 1631  $\nu(-\text{HC}=\text{N})$ ; 3305  $\nu(\text{NH}_2)$ ; 3427, 1413, 1381  $\nu(-\text{COO}^-)$ , ( $-\text{COO}^-$ )  $\nu_{\text{asy}}$ , ( $-\text{COO}^-$ )  $\nu_{\text{sy}}$ ; 503  $\nu(\text{M}-\text{O})$ ; 433  $\nu(\text{M}-\text{N})$ . MS  $m/z$  (%): 521  $[\text{M}+1]^+$ .  $\lambda_{\text{max}}$  ( $\text{cm}^{-1}$ ) in DMF, 10,246, 29,240.  $\mu_{\text{eff}}$  (BM): 1.89.

$[\text{Cu}(\text{L})(\text{Val})_2]$ . Yield: 68%. Anal. Calc. for  $C_{26}H_{35}N_5O_6\text{Cu}$ : Cu, 11.0; C, 54.1; H, 6.1; N, 12.1 (%); Found: Cu, 10.7; C, 53.8; H, 6.0; N, 11.7 (%). IR (KBr pellet,  $\text{cm}^{-1}$ ): 1645  $\nu(\text{C}=\text{O})$ ; 1629  $\nu(-\text{HC}=\text{N})$ ; 3310  $\nu(\text{NH}_2)$ ; 3392, 1406, 1386  $\nu(-\text{COO}^-)$ , ( $-\text{COO}^-$ )  $\nu_{\text{asy}}$ , ( $-\text{COO}^-$ )  $\nu_{\text{sy}}$ ; 501  $\nu(\text{M}-\text{O})$ ; 428  $\nu(\text{M}-\text{N})$ . MS  $m/z$  (%): 578  $[\text{M}+1]^+$ .  $\lambda_{\text{max}}$  ( $\text{cm}^{-1}$ ) in DMF, 11,236, 29,586.  $\mu_{\text{eff}}$  (BM): 1.93.

$[\text{Co}(\text{L})(\text{Gly})_2]$ . Yield: 69%. Anal. Calc. for  $C_{20}H_{23}N_5O_6\text{Co}$ : Co, 12.1; C, 49.2; H, 4.7; N, 14.3 (%); Found: Co, 11.8; C, 48.7; H, 4.4; N, 14.1 (%). IR (KBr pellet,  $\text{cm}^{-1}$ ): 1647  $\nu(\text{C}=\text{O})$ ; 1595  $\nu(-\text{HC}=\text{N})$ ; 3305  $\nu(\text{NH}_2)$ ; 3404, 1417, 1390  $\nu(-\text{COO}^-)$ , ( $-\text{COO}^-$ )  $\nu_{\text{asy}}$ , ( $-\text{COO}^-$ )  $\nu_{\text{sy}}$ ; 501  $\nu(\text{M}-\text{O})$ ; 434  $\nu(\text{M}-\text{N})$ . MS  $m/z$  (%): 488  $[\text{M}+1]^+$ .  $\lambda_{\text{max}}$  ( $\text{cm}^{-1}$ ) in DMF, 12,300, 15,924, 37,313.  $\mu_{\text{eff}}$  (BM): 4.48.

$[\text{Co}(\text{L})(\text{Ala})_2]$ . Yield: 53%. Anal. Calc. for  $C_{22}H_{27}N_5O_6\text{Co}$ : Co, 11.4; C, 51.2; H, 5.3; N, 13.6 (%); Found: Co, 11.1; C, 50.9; H, 5.0; N, 13.2



**Scheme 1.** Synthetic route of Schiff base and its metal complexes.

(%). IR (KBr pellet,  $\text{cm}^{-1}$ ): 1645  $\nu(\text{C}=\text{O})$ ; 1597  $\nu(-\text{HC}=\text{N})$ ; 3310  $\nu(\text{NH}_2)$ ; 3429, 1419, 1382  $\nu(-\text{COO}^-)$ ,  $(-\text{COO}^-) \nu_{\text{asy}}$ ,  $(-\text{COO}^-) \nu_{\text{sy}}$ ; 500  $\nu(\text{M}-\text{O})$ ; 428  $\nu(\text{M}-\text{N})$ . MS  $m/z$  (%): 517  $[\text{M}+1]^+$ .  $\lambda_{\text{max}}$  ( $\text{cm}^{-1}$ ) in DMF, 11,099, 12,920, 29,411.  $\mu_{\text{eff}}$  (BM): 4.92.

[Co(L)(Val)<sub>2</sub>]. Yield: 78%. Anal. Calc. for  $\text{C}_{26}\text{H}_{35}\text{N}_5\text{O}_6\text{Co}$ : Co, 10.3; C, 54.5; H, 6.2; N, 12.2 (%); Found: Co, 10.1; C, 54.1; H, 5.9; N, 11.8 (%). IR (KBr pellet,  $\text{cm}^{-1}$ ): 1641  $\nu(\text{C}=\text{O})$ ; 1628  $\nu(-\text{HC}=\text{N})$ ; 3304  $\nu(\text{NH}_2)$ ; 3427, 1413, 1381  $\nu(-\text{COO}^-)$ ,  $(-\text{COO}^-) \nu_{\text{asy}}$ ,  $(-\text{COO}^-) \nu_{\text{sy}}$ ; 501  $\nu(\text{M}-\text{O})$ ; 436  $\nu(\text{M}-\text{N})$ . MS  $m/z$  (%): 573  $[\text{M}+1]^+$ .  $\lambda_{\text{max}}$  ( $\text{cm}^{-1}$ ) in DMF, 12,422, 16,977, 29,450.  $\mu_{\text{eff}}$  (BM): 4.89.

[Ni(L)(Gly)<sub>2</sub>]. Yield: 73%. Anal. Calc. for  $\text{C}_{20}\text{H}_{23}\text{N}_5\text{O}_6\text{Ni}$ : Ni, 12.0; C, 49.2; H, 4.7; N, 14.3 (%); Found: Ni, 11.7; C, 48.8; H, 4.4; N, 13.9 (%). IR (KBr pellet,  $\text{cm}^{-1}$ ): 1647  $\nu(\text{C}=\text{O})$ ; 1595  $\nu(-\text{HC}=\text{N})$ ; 3345  $\nu(\text{NH}_2)$ ; 3442, 1411, 1395  $\nu(-\text{COO}^-)$ ,  $(-\text{COO}^-) \nu_{\text{asy}}$ ,  $(-\text{COO}^-) \nu_{\text{sy}}$ ; 503  $\nu(\text{M}-\text{O})$ ; 433  $\nu(\text{M}-\text{N})$ . MS  $m/z$  (%): 488  $[\text{M}+1]^+$ .  $\lambda_{\text{max}}$  ( $\text{cm}^{-1}$ ) in DMF, 12,453, 13,228, 36,364.  $\mu_{\text{eff}}$  (BM): 3.07.

[Ni(L)(Ala)<sub>2</sub>]. Yield: 51%. Anal. Calc. for  $\text{C}_{22}\text{H}_{27}\text{N}_5\text{O}_6\text{Ni}$ : Ni, 11.4; C, 51.2; H, 5.3; N, 13.6 (%); Found: Ni, 11.1; C, 51.8; H, 5.1; N, 13.2 (%). IR (KBr pellet,  $\text{cm}^{-1}$ ): 1647  $\nu(\text{C}=\text{O})$ ; 1629  $\nu(-\text{HC}=\text{N})$ ; 3315  $\nu(\text{NH}_2)$ ; 3427, 1413, 1381  $\nu(-\text{COO}^-)$ ,  $(-\text{COO}^-) \nu_{\text{asy}}$ ,  $(-\text{COO}^-) \nu_{\text{sy}}$ ; 501  $\nu(\text{M}-\text{O})$ ; 435  $\nu(\text{M}-\text{N})$ . MS  $m/z$  (%): 517  $[\text{M}+1]^+$ .  $\lambda_{\text{max}}$  ( $\text{cm}^{-1}$ ) in DMF, 12,360, 13,774, 29,326.  $\mu_{\text{eff}}$  (BM): 3.14.

[Ni(L)(Val)<sub>2</sub>]. Yield: 71%. Anal. Calc. for  $\text{C}_{26}\text{H}_{35}\text{N}_5\text{O}_6\text{Ni}$ : Ni, 10.3; C, 54.6; H, 6.2; N, 12.2 (%); Found: Ni, 9.9; C, 54.1; H, 5.9; N, 11.7 (%). IR (KBr pellet,  $\text{cm}^{-1}$ ): 1647  $\nu(\text{C}=\text{O})$ ; 1620  $\nu(-\text{HC}=\text{N})$ ; 3317  $\nu(\text{NH}_2)$ ; 3427, 1421, 1373  $\nu(-\text{COO}^-)$ ,  $(-\text{COO}^-) \nu_{\text{asy}}$ ,  $(-\text{COO}^-) \nu_{\text{sy}}$ ; 503  $\nu(\text{M}-\text{O})$ ; 428  $\nu(\text{M}-\text{N})$ . MS  $m/z$  (%): 573  $[\text{M}+1]^+$ .  $\lambda_{\text{max}}$  ( $\text{cm}^{-1}$ ) in DMF, 12,315, 17,211, 29,411.  $\mu_{\text{eff}}$  (BM): 3.17.

[Zn(L)(Gly)<sub>2</sub>]. Yield: 81%. Anal. Calc. for  $\text{C}_{20}\text{H}_{23}\text{N}_5\text{O}_6\text{Zn}$ : Zn, 13.2; C, 48.5; H, 4.7; N, 14.2 (%); Found: Zn, 12.7; C, 48.2; H, 4.3; N, 13.9 (%). IR (KBr pellet,  $\text{cm}^{-1}$ ): 1646  $\nu(\text{C}=\text{O})$ ; 1595  $\nu(-\text{HC}=\text{N})$ ; 3310  $\nu(\text{NH}_2)$ ; 3442, 1411, 1393  $\nu(-\text{COO}^-)$ ,  $(-\text{COO}^-) \nu_{\text{asy}}$ ,  $(-\text{COO}^-) \nu_{\text{sy}}$ ; 503  $\nu(\text{M}-\text{O})$ ; 430  $\nu(\text{M}-\text{N})$ . <sup>1</sup>H NMR ( $\delta$ ): (aromatic) 6.5–7.1 (m); (C–CH<sub>3</sub>) 2.3 (s); (N–CH<sub>3</sub>) 3.1(s); (CH=N) 9.6(s). MS  $m/z$  (%): 495  $[\text{M}+1]^+$ .  $\lambda_{\text{max}}$  ( $\text{cm}^{-1}$ ) in DMF, 29,412, 36,232.  $\mu_{\text{eff}}$  (BM): Diamagnetic.

[Zn(L)(Ala)<sub>2</sub>]. Yield: 72%. Anal. Calc. for  $\text{C}_{22}\text{H}_{27}\text{N}_5\text{O}_6\text{Zn}$ : Zn, 12.5; C, 50.5; H, 5.2; N, 13.4 (%); Found: Zn, 12.2; C, 50.1; H, 4.8; N, 13.1 (%). IR (KBr pellet,  $\text{cm}^{-1}$ ): 1646  $\nu(\text{C}=\text{O})$ ; 1625  $\nu(-\text{HC}=\text{N})$ ; 3302  $\nu(\text{NH}_2)$ ; 3425, 1413, 1381  $\nu(-\text{COO}^-)$ ,  $(-\text{COO}^-) \nu_{\text{asy}}$ ,  $(-\text{COO}^-) \nu_{\text{sy}}$ ; 503  $\nu(\text{M}-\text{O})$ ; 435  $\nu(\text{M}-\text{N})$ . <sup>1</sup>H NMR ( $\delta$ ): (aromatic) 6.5–7.3 (m); (C–CH<sub>3</sub>) 2.3 (s); (N–CH<sub>3</sub>) 3.2(s); (CH=N) 9.7(s). MS  $m/z$  (%): 523  $[\text{M}+1]^+$ .  $\lambda_{\text{max}}$  ( $\text{cm}^{-1}$ ) in DMF, 29,498, 35,482.  $\mu_{\text{eff}}$  (BM): Diamagnetic.

[Zn(L)(Val)<sub>2</sub>]. Yield: 67%. Anal. Calc. for C<sub>26</sub>H<sub>35</sub>N<sub>5</sub>O<sub>6</sub>Zn: Zn, 11.3; C, 53.9; H, 6.1; N, 12.1 (%); Found: Zn, 10.9; C, 53.3; H, 5.8; N, 11.7 (%). IR (KBr pellet, cm<sup>-1</sup>): 1647 ν(C=O); 1620 ν(–HC=N); 3317 ν(NH<sub>2</sub>); 3427, 1421, 1386 ν((COO<sup>-</sup>), (–COO<sup>-</sup>)<sub>asy</sub>, (–COO<sup>-</sup>)<sub>sy</sub>); 503 ν(M–O); 428 ν(M–N). <sup>1</sup>H NMR (δ): (aromatic) 6.5–7.2 (m); (C–CH<sub>3</sub>) 2.4 (s); (N–CH<sub>3</sub>) 3.3(s); (CH=N) 9.6(s). MS *m/z* (%): 579 [M+1]<sup>+</sup>. λ<sub>max</sub> (cm<sup>-1</sup>) in DMF, 29,325, 35,335. μ<sub>eff</sub> (BM): Diamagnetic.

#### 2.4. DNA binding experiments

The interaction between metal complexes and DNA was studied by electronic absorption, viscosity and electrochemical methods. Disodium salt of calf thymus DNA was stored at 4 °C. All the experiments involving the interaction of the complexes with calf thymus (CT) DNA were carried out in Tris–HCl buffer (50 mM Tris–HCl, pH 7.2) containing 5% DMF at room temperature. Solution of CT DNA in the buffer gave a ratio of UV absorbance at 260 and 280 nm, A<sub>260</sub>/A<sub>280</sub> of ca. 1.89:1, indicating that the CT DNA was sufficiently free from protein [18]. The concentration of DNA was measured by using its extinction coefficient at 260 nm (6600 M<sup>-1</sup> cm<sup>-1</sup>) after 1:100 dilution. Stock solutions were stored at 4 °C and used not more than 4 days. Doubly distilled water was used to prepare solutions. Concentrated stock solutions of the complexes were prepared by dissolving the complexes in DMF and diluting properly with the corresponding buffer to the required concentration for all the experiments.

The electronic spectra of the complexes were recorded before and after the addition of DNA in the presence of 5 mM Tris–HCl/50 mM NaCl buffer (pH 7.2). The intrinsic binding constant for the interaction of complex with DNA was obtained from absorption data. A fixed concentration value of complex (10 μM) was titrated with increasing amounts of DNA over the range of 20–150 μM. The equilibrium binding constant (K<sub>b</sub>) values for the interaction of the complexes with DNA were obtained from the absorption spectral titration data using the following equation

$$[\text{DNA}]/(\varepsilon_a - \varepsilon_f) = [\text{DNA}]/(\varepsilon_b - \varepsilon_f) + 1/K_b(\varepsilon_b - \varepsilon_f) \quad (1)$$

where ε<sub>a</sub> the extinction coefficient observed for the charge transfer absorption at a given DNA concentration, ε<sub>f</sub>, the extinction coefficient of the complex free in solution, ε<sub>b</sub>, the extinction coefficient of the complex when fully bound to DNA, K<sub>b</sub>, the intrinsic binding constant and [DNA], the concentration in nucleotides. A plot of [DNA]/(ε<sub>a</sub> – ε<sub>f</sub>) versus [DNA], gives K<sub>b</sub> as the ratio of the slope to the intercept.

Cyclic voltammetry studies were performed on a CHI 620C electrochemical analyzer with three electrode system of glassy carbon as the working electrode, a platinum wire as auxiliary electrode and Ag/AgCl as the reference electrode. Solutions were deoxygenated by purging with N<sub>2</sub> prior to measurements. Viscosity experiments were carried on an Ostwald viscometer, immersed in a thermostated water-bath maintained at a constant temperature at 30.0 ± 0.1 °C. CT DNA samples of approximately 0.5 mM were prepared by sonicating in order to minimize complexities arising from CT DNA flexibility [19]. Flow time was measured with a digital stopwatch three times for each sample and an average flow time was calculated. Data were presented as (η/η<sub>0</sub>)<sup>1/3</sup> versus the concentration of the metal(II) complexes, where η is the viscosity of CT DNA solution in the presence of complex, and η<sub>0</sub> is the viscosity of CT DNA solution in the absence of complex. Viscosity values were calculated after correcting the flow time of buffer alone (t<sub>0</sub>), η = (t – t<sub>0</sub>)/t<sub>0</sub> [20].

#### 2.5. Interaction with pUC19 DNA plasmid DNA

The extent of pUC19 DNA cleavage in presence of activating agent AH<sub>2</sub> (ascorbic acid), and two radical scavengers DMSO (hydroxyl radical scavenger) and NaN<sub>3</sub> (singlet oxygen scavenger) was monitored using agarose gel electrophoresis. In reactions using super coiled pUC19 plasmid DNA Form I (10 μM) in Tris–HCl buffer (50 mM) with 50 mM NaCl (pH 7.2) which was treated with the metal complex and ascorbic acid (10 μM) followed by dilution with the Tris–HCl buffer to a total volume of 20 μL. The samples were incubated for 1 h at 37 °C. A loading buffer containing 0.25% bromophenol blue was added and electrophoresis was performed at 40 V for each hour in Tris–Acetate–EDTA (TAE) buffer using 1% agarose gel containing 1.0 μg/mL ethidium bromide. The cleavage efficiency was measured by determining the ability of the complex to convert the super coiled (SC) DNA to nicked circular form (NC) and linear form (LC). Inhibition reactions were carried out by prior incubation of the pUC19 DNA (10 mM) with DMSO (4 μL).

#### 2.6. Antimicrobial studies

##### 2.6.1. Antibacterial activity

National Committee for Clinical Laboratory Standard (NCCLS) approved standard nutrient agar was used as medium for testing the activity of microorganisms as antibacterial agents [21]. For preparing the agar media, 3 g of beef extract, 5 g of peptone, 5 g of yeast extract and 5 g of sodium chloride were dissolved in 1000 mL of distilled water in a clean conical flask. The pH of the solution was maintained at 7. The solution was boiled to dissolve the medium completely and sterilized by autoclaving at 15 lbs pressure (121 °C) for 30 min. After sterilization, 20 mL of media was poured into the sterilized petri plates. These petri plates were kept at room temperature for sometime. After few minutes the medium got solidified in the plates. Then, it was inoculated with microorganisms using sterile swabs. The stock solutions were prepared by dissolving the compounds in appropriate solvents.

In a typical procedure [18], the antibacterial activities of the compounds were evaluated by the disc diffusion method against the bacterial microorganisms. The 5 mm diameter and 1 mm thickness of the disc was filled with the test solutions using a micropipette and the plates were incubated at 37 °C for 24 h. During this period, the test solution was diffused and affected the growth of the inoculated bacteria. The zone of inhibition, developed on the plate was measured.

##### 2.6.2. Antifungal activity

NCCLS approved standard potato dextrose agar was used as medium for antifungal activity by disc diffusion method [18]. For preparing the agar media, 200 g of potato extract, 20 g of agar and 20 g of dextrose were dissolved in 1000 mL of distilled water in a clean conical flask. The solution was boiled to dissolve the medium completely and sterilized by autoclaving at 15 lbs pressure (121 °C) for 30 min. After sterilization, 20 mL of media was poured into the sterilized petri plates. These petri plates were kept at room temperature for sometime. After few minutes the medium got solidified in the plates. Then, it was inoculated with microorganisms using sterile swabs. In a typical procedure [18], the antifungal activities of the compounds were evaluated by the disc diffusion method against the fungal microorganisms. The 5 mm diameter and 1 mm thickness of the disc was filled with the test solution using a micropipette and the plates were incubated at 37 °C for 72 h. During this period, the test solution was diffused and affected the growth of the inoculated fungi. After 36 h of incubation at 37 °C, the diameter of the inhibition was measured. Compounds showing promising antibacterial/antifungal activity were

selected for minimum inhibitory concentration studies. The minimum inhibitory concentration was determined by assaying at concentration of compounds along with standards at the same concentration. Minimum inhibitory concentration (MIC) is the lowest concentration of an antimicrobial compound, inhibiting the visible growth of microorganisms after overnight incubation. Minimum inhibitory concentrations are important in diagnostic laboratories to confirm resistance of microorganisms to antimicrobial agents and also to monitor the activity of new antimicrobial agents.

### 2.7. Antioxidant property

Hydroxyl radicals were generated in aqueous media through the Fenton-type reaction [22,23]. The aliquots of reaction mixture (3 mL) contained 1.0 mL of 0.10 mmol aqueous safranin, 1 mL of 1.0 mmol aqueous EDTA–Fe(II), 1 mL of 3% aqueous H<sub>2</sub>O<sub>2</sub>, and a series of quantitative microaddition of solutions of the test compound. A sample without the tested compound was used as the control. The reaction mixtures were incubated at 37 °C for 30 min in a water bath. The absorbance was then measured at 520 nm. All the tests were run in triplicate and are expressed as the mean and standard deviation (SD) [24]. The scavenging effect for OH<sup>•</sup> was calculated from the following expression:

$$\text{Scavenging ratio (\%)} = [(A_i - A_o)/(A_c - A_o)] \times 100\% \quad (2)$$

where  $A_i$  is the absorbance in the presence of the test compound;  $A_o$  is the absorbance of the blank in the absence of the test compound;  $A_c$  is the absorbance in the absence of the test compound, EDTA–Fe(II) and H<sub>2</sub>O<sub>2</sub>.

## 3. Results and discussion

The Schiff base ligand and the Co(II), Cu(II), Ni(II), and Zn(II) complexes have been synthesized and characterized by spectral and elemental analytical data. They are found to be air stable. The ligand is soluble in common organic solvents and all the complexes are freely soluble in DMF and DMSO.

### 3.1. Physical measurements

The elemental analytical results for the metal complexes are in good agreement with the calculated values showing that the complexes have the stoichiometry of the type [MLA<sub>2</sub>]. Here L is a Schiff-base ligand which is prepared by the condensation of 4-aminoantipyrine with furfural which acts as a bidentate ligand and amino acids (A) such as glycine, alanine and valine, used as co-ligands. The metal(II) complexes were dissolved in DMF and the molar conductivities of 10<sup>-3</sup> M of their solution at room temperature were measured. The lower conductance values (15–30 Ω<sup>-1</sup> cm<sup>2</sup> mol<sup>-1</sup>) of the complexes support their non-electrolytic nature of the compounds.

The measured magnetic moment values for [Cu(L)(Gly)<sub>2</sub>], [Cu(L)(Ala)<sub>2</sub>] and [Cu(L)(Val)<sub>2</sub>] complexes are 1.87, 1.89 and 1.93 BM respectively. These values are also closely agreed with the magnetic moment values which are calculated from the EPR spectral studies of the above complexes. The observed magnetic moment values indicate the monomeric nature of the copper complexes. [Co(L)(Gly)<sub>2</sub>], [Co(L)(Ala)<sub>2</sub>] and [Co(L)(Val)<sub>2</sub>], complexes reported herein have magnetic moment values, 4.84, 4.92 and 4.89 BM at room temperature respectively. The magnetic moment values of all above Co(II) complexes (normal range for octahedral Co(II) complexes is 4.3–5.2 BM) indicate that they adopt an octahedral geometry.

The measured magnetic moment values for [Ni(L)(Gly)<sub>2</sub>], [Ni(L)(Ala)<sub>2</sub>] and [Ni(L)(Val)<sub>2</sub>] complexes are 3.07, 3.14 and 3.17 BM respectively, which are in the normal range of nickel(II) complexes having magnetic moments between  $\mu_{\text{eff}}$  2.9 and 3.4 BM. This indicates that the complex of Ni(II) ion is six coordinated and probably octahedral indicating a small but definite orbital contribution to the magnetic moment.

### 3.2. Electronic spectra

The UV–Vis spectra of L and its mixed ligand complexes were recorded in DMF solution at room temperature. The bands appearing at low energy side are attributed to n– $\pi^*$  transitions which are associated with the azomethine chromophore. The bands at higher energy arise from  $\pi$ – $\pi^*$  transitions within the phenyl rings [25]. The absorption bands of the complexes are shifted to longer wavelength region compared to those of the ligand [26,27]. All the complexes show the high energy absorption bands in the region 35,211–37,313 cm<sup>-1</sup>. This transition may be attributed to the charge transfer band. The electronic spectra of [Cu(L)(Gly)<sub>2</sub>], [Cu(L)(Ala)<sub>2</sub>] and [Cu(L)(Val)<sub>2</sub>] complexes display the d–d transition bands in the region 11,001, 10,246 and 11,236 cm<sup>-1</sup>, respectively, which are due to <sup>2</sup>E<sub>g</sub> → <sup>2</sup>T<sub>2g</sub> transition. This d–d transition band strongly favours a distorted octahedral geometry around the metal ion. Electronic spectra of [Co(L)(Gly)<sub>2</sub>], [Co(L)(Ala)<sub>2</sub>] and [Co(L)(Val)<sub>2</sub>] complexes display the d–d transition bands in the region 12,300, 15,924 and 37,313 cm<sup>-1</sup>, 11,099, 12,920 and 29,411 cm<sup>-1</sup>, 12,422, 16,977 and 29,450 cm<sup>-1</sup> which are assigned to <sup>4</sup>T<sub>1g</sub>(F) → <sup>4</sup>T<sub>2g</sub>(F), <sup>4</sup>T<sub>1g</sub>(F) → <sup>4</sup>A<sub>2g</sub>(F) and <sup>4</sup>T<sub>1g</sub>(F) → <sup>4</sup>T<sub>2g</sub>(P) transitions, respectively. These transitions correspond to the octahedral geometry, supported by their magnetic susceptibility values (4.84–4.92 BM).

The absorption spectra of [Ni(L)(Gly)<sub>2</sub>], [Ni(L)(Ala)<sub>2</sub>] and [Ni(L)(Val)<sub>2</sub>] complexes display three d–d bands at 12,453, 13,228 and 36,364 cm<sup>-1</sup>, 12,360, 13,774 and 29,326, 14,577, 17,211 and 29,411 cm<sup>-1</sup> respectively. These correspond to <sup>3</sup>A<sub>2g</sub>(F) → <sup>3</sup>T<sub>2g</sub>(F), <sup>3</sup>A<sub>2g</sub>(F) → <sup>3</sup>T<sub>1g</sub>(F) and <sup>3</sup>A<sub>2g</sub>(F) → <sup>3</sup>T<sub>1g</sub>(P) transitions, respectively and being the characteristic of an octahedral geometry. This geometry is further supported by their magnetic susceptibility values (3.07–3.17 BM). The Zn(II) complexes are diamagnetic and also exhibit INCT bands. According to the empirical formulae, an octahedral geometry is proposed for Zn(II) complexes.

#### 3.2.1. <sup>1</sup>H NMR and <sup>13</sup>C NMR spectra

The typical <sup>1</sup>H NMR spectra of L and the zinc(II) complex were shown in Fig. S1(a and b). <sup>1</sup>H NMR spectrum of the Schiff base ligand shows peaks at 6.6–7.4  $\delta$  which are attributed to phenyl multiplet of Schiff base ligand (obtained from the condensation of 4-aminoantipyrine and furfuraldehyde). The ligand also shows the following signals: C–CH<sub>3</sub> 2.3–2.4  $\delta$ (s), N–CH<sub>3</sub> 3.1–3.3  $\delta$ (s); CH=N 9.3  $\delta$ (s) and 6.62, 6.94 and 7.83  $\delta$  for furfurylidene moiety. The azomethine proton –CH=N signals in the spectra of the zinc complexes are shifted to down field (9.6  $\delta$ ) compared to the free ligands, suggesting deshielding of azomethine group due to the coordination with metal ion. There is no appreciable change in all other signals of the complexes. The peak at 11  $\delta$  is attributed to the –COOH of amino acid (glycine/alanine/valine). The absence of this peak noted for the zinc complexes confirms the loss of the COOH proton of amino acid moiety due to complexation. The peak at 5.1  $\delta$  is attributed to the –NH<sub>2</sub> of amino acid (glycine/alanine/valine), but in the zinc complex, it is shifted to down field region which indicates amino group is involved in complexation. <sup>13</sup>C NMR spectrum of L shows aromatic carbons at 116–139 ppm. It also shows C–CH<sub>3</sub> at 14.8  $\delta$ , N–CH<sub>3</sub> at 40.2  $\delta$ , –COO<sup>-</sup> at 171  $\delta$ , –CH=N at 163  $\delta$  and 149  $\delta$  for furfurylidene moiety. From the <sup>13</sup>C NMR spectra of zinc complexes, it can be known that –C=O

and  $-\text{CH}=\text{N}$  groups are involved in complexation through down field shift. There is no appreciable change in other signals of the complex.

### 3.3. IR spectra

The coordination mode and sites of the ligand to the metal ions were investigated by comparing the infrared spectra of the free ligand with its metal complexes. The IR spectrum shows a band at  $1665\text{ cm}^{-1}$  for the free ligand (L), assigned to  $\nu_{\text{C}=\text{O}}$  of 4-aminoantipyrine, shifted towards lower values around  $1641\text{--}1653\text{ cm}^{-1}$  indicating the coordination of the carbonyl oxygen atom of the 4-aminoantipyrine derived Schiff base ligand to metal ion. The spectrum of free ligand shows a band in the region  $1645\text{ cm}^{-1}$ , a characteristic feature of the  $\nu_{\text{C}=\text{N}}$  (azomethine) stretching mode indicating the formation of the Schiff base product originating from amino and carbonyl groups of the starting reagents (4-aminoantipyrine and furfural). This band is shifted towards lower frequencies in the spectra of metal complexes ( $1595\text{--}1637\text{ cm}^{-1}$ ) compared to the above Schiff base ligand indicating the involvement of the azomethine nitrogen in coordination with metal ion. Moreover, the coordination of the co-ligand to the metal centre via the carboxylic group can also be obvious from the difference of maxima positions as observed for  $\nu_{\text{sy},(\text{COO}^-)}$  and  $\nu_{\text{asy},(\text{COO}^-)}$ . The bands are observed at  $1390$  and  $1427\text{ cm}^{-1}$  respectively for a free amino acid ligand, For comparison, the  $\nu_{\text{sy},(\text{COO}^-)}$  and  $\nu_{\text{asy},(\text{COO}^-)}$  display bands at  $1370\text{--}1395$  and  $1406\text{--}1421\text{ cm}^{-1}$ , respectively for all the metal complexes. These results reveal that the amino acid ligand is involved in the coordination through the carboxyl group. In addition to it, the coordination of the co-ligand to the metal centre via the amino group is observed. The band is observed at  $3340\text{ cm}^{-1}$  for the amino group of free amino acid ligand but it is shifted to lower frequency region ( $30\text{ cm}^{-1}$ ) that indicates amino group of amino acid is involved in complexation. Conclusive evidence of the bonding is also shown by the observation that new bands in the spectra of all metal complexes appearing in the low frequency regions at  $501\text{--}503\text{ cm}^{-1}$  and  $430\text{--}450\text{ cm}^{-1}$  which are characteristic to the  $\nu_{(\text{M}-\text{O})}$  and  $\nu_{(\text{M}-\text{N})}$  stretching vibrations respectively that are not observed in the spectrum of free ligand.

### 3.4. Mass spectra

The FAB mass spectrum of synthesized **L** is recorded and the obtained molecular ion peaks confirm the proposed formulae. The mass spectrum of L shows M+1 peak at  $m/z$  282 (91.71%) corresponding to  $(\text{C}_{16}\text{H}_{15}\text{N}_3\text{O}_2)^+$  ion. Also the spectrum exhibits the fragments at  $m/z$  214, 202, 188, 172 and 157 corresponding to  $[\text{C}_{12}\text{H}_{12}\text{N}_3\text{O}]^+$ ,  $[\text{C}_{11}\text{H}_{11}\text{N}_3\text{O}]^+$ ,  $[\text{C}_{11}\text{H}_{11}\text{N}_2\text{O}]^+$ ,  $[\text{C}_{10}\text{H}_8\text{N}_2\text{O}]^+$  and  $[\text{C}_{10}\text{H}_8\text{N}_2]^+$  respectively (Fig. 4(a)). The spectrum of  $[\text{Co}(\text{L})(\text{Gly})_2]^+$  complex shows molecular ion peak at  $m/z$  488 [M+1] which is equivalent to its molecular weight. The  $[\text{Co}(\text{L})(\text{Gly})_2]$  complex gives fragment ion peaks at  $m/z$  471, 428, 384, 326 and 282 corresponding to  $[\text{C}_{20}\text{H}_{21}\text{N}_4\text{O}_6\text{Co}]^+$ ,  $[\text{C}_{17}\text{H}_{14}\text{N}_4\text{O}_6\text{Co}]^+$ ,  $[\text{C}_{16}\text{H}_{14}\text{N}_4\text{O}_4\text{Co}]^+$ ,  $[\text{C}_{16}\text{H}_{14}\text{N}_4\text{O}_4]^+$  and  $[\text{C}_{15}\text{H}_{14}\text{N}_4\text{O}_2]^+$  ions respectively. The spectrum of  $[\text{Cu}(\text{L})(\text{Ala})_2]^+$  complex shows molecular ion peak at  $m/z$  521 [M+1] which is equivalent to its molecular weight. The  $[\text{Cu}(\text{L})(\text{Ala})_2]$  complex gives fragment ion peaks at  $m/z$  504, 491, 448, 385, 341, 325 and 281 corresponding to  $[\text{C}_{22}\text{H}_{25}\text{N}_4\text{O}_6\text{Cu}]^+$ ,  $[\text{C}_{21}\text{H}_{24}\text{N}_4\text{O}_6\text{Cu}]^+$ ,  $[\text{C}_{18}\text{H}_{17}\text{N}_4\text{O}_6\text{Cu}]^+$ ,  $[\text{C}_{18}\text{H}_{17}\text{N}_4\text{O}_6]^+$ ,  $[\text{C}_{17}\text{H}_{17}\text{N}_4\text{O}_4]^+$ ,  $[\text{C}_{17}\text{H}_{15}\text{N}_3\text{O}_4]^+$  and  $[\text{C}_{16}\text{H}_{15}\text{N}_3\text{O}_2]^+$  ions respectively. The spectrum of  $[\text{Zn}(\text{L})(\text{Val})_2]^+$  complex shows molecular ion peak at  $m/z$  579 [M+1] which is equivalent to its molecular weight. Moreover, the  $[\text{Zn}(\text{L})(\text{Val})_2]$  complex gives fragment ion peaks at  $m/z$  562, 549, 506, 441, 426, 382 and 339 corresponding to  $[\text{C}_{26}\text{H}_{33}\text{N}_4\text{O}_6\text{Zn}]^+$ ,  $[\text{C}_{25}\text{H}_{32}\text{N}_4\text{O}_6\text{Zn}]^+$ ,  $[\text{C}_{22}\text{H}_{25}\text{N}_4\text{O}_6\text{Zn}]^+$ ,  $[\text{C}_{22}\text{H}_{25}\text{N}_4\text{O}_6]^+$ ,  $[\text{C}_{21}\text{H}_{22}\text{N}_4\text{O}_6]^+$ ,  $[\text{C}_{20}\text{H}_{22}\text{N}_4\text{O}_4]^+$  and  $[\text{C}_{17}\text{H}_{15}\text{N}_4\text{O}_4]^+$  ions respectively. All these

fragments lead to the formation of the species  $[\text{M}(\text{L})(\text{A})_2]^+$  which further undergoes de-metallation to yield the species  $[\text{L}]^+$  giving the fragment ion peak at  $m/z$  282. The  $m/z$  of all the fragments of ligands and their complexes confirm the stoichiometry of the complexes as  $[\text{M}(\text{L})(\text{A})_2]$ .

### 3.5. EPR spectra

Mixed ligand complex is found to be interesting due to the fact that the arrangement of ligand atoms around Cu(II) is found to change as one goes from the solid to the solution state. Hence to obtain further information about the stereochemistry and to interpret bonding parameters, the EPR spectra of  $[\text{Cu}(\text{L})(\text{Gly})_2]$ ,  $[\text{Cu}(\text{L})(\text{Ala})_2]$  and  $[\text{Cu}(\text{L})(\text{Val})_2]$  complexes have been studied. The EPR spectra of copper complexes were recorded in DMSO solution both at room temperature (RT) and at liquid nitrogen temperature (LNT) and are given in Fig. S2(a and b) and the spectral data are given in Table 1. The spectrum at RT shows one intense absorption band in the high field and is isotropic due to the tumbling motion of the molecules. However,  $[\text{Cu}(\text{L})(\text{Gly})_2]$ ,  $[\text{Cu}(\text{L})(\text{Ala})_2]$  and  $[\text{Cu}(\text{L})(\text{Val})_2]$  complexes at LNT show well resolved peaks with low field region. The anisotropic data ( $g_{\parallel}$  values of 2.3336, 2.3759 and 2.3797 and  $g_{\perp}$  values of 2.060, 2.0795 and 2.1665) have been obtained from frozen solution spectra at 77 K which are well resolved at low field.  $g$  tensor values of Cu(II) complexes can be used to derive the ground state of the complexes. The observed values,  $g_{\parallel} > g_{\perp} > g_e$  and  $A_{\parallel} > A_{\perp}$  reveal that the unpaired electron of Cu(II) ion lies predominantly in the  $d_{x^2-y^2}$  orbital giving  $^2E_g$  as ground state. From the values of  $g$  factors, the geometric parameter  $G$ , representing a measure of exchange interaction between Cu(II) centres in polycrystalline compound can be determined by using the formula:

$$G = (g_{\parallel} - 2)/(g_{\perp} - 2) \quad (3)$$

If  $G > 4.0$ , the local tetragonal axes are aligned parallel or only slightly misaligned. If  $G < 4.0$ , significant exchange coupling is present and the misaligned is appreciable. The observed values for the exchange interaction parameter for  $[\text{Cu}(\text{L})(\text{Gly})_2]$ ,  $[\text{Cu}(\text{L})(\text{Ala})_2]$  and  $[\text{Cu}(\text{L})(\text{Val})_2]$  complexes are 5.8170, 4.8847 and 5.4938  $G$  which suggest that the local tetragonal axes are aligned parallel or slightly misaligned and the unpaired electron is present in the  $d_{x^2-y^2}$  orbital. This result also indicates that the exchange coupling effects are not operative in the present complexes [28]. In this study,  $g_{\parallel}$  value is greater than 2.33 suggesting the conformity with the presence of mixed copper–nitrogen and copper–oxygen bonding to the chelates.

The empirical ratio of  $g_{\parallel}|A_{\parallel}|$  is frequently used to evaluate distortion in copper(II) complexes. The ratio is close to 100 indicates a roughly square-planar structure around the Cu(II) ion and the values from 170 to 250 are indicative of distorted tetrahedral geometry. If the ratio is in between 110 and 170, it indicates nearly octahedral environment around Cu(II) ion with small distortion. The observed  $g_{\parallel}|A_{\parallel}|$  values for the  $[\text{Cu}(\text{L})(\text{Gly})_2]$ ,  $[\text{Cu}(\text{L})(\text{Ala})_2]$  and  $[\text{Cu}(\text{L})(\text{Val})_2]$  complexes are 137, 158 and 132 respectively which suggest that all the above complexes are having distorted octahedral structure.

Electron paramagnetic resonance and optical spectra have been used to determine the covalent bonding parameters for the Cu(II) ion in various environments. Since there has been wide interest in the nature of bonding parameters in the system, the simplified molecular orbital theory [29] is adopted to calculate the bonding coefficients such as  $\alpha^2$  (covalent in-plane  $\sigma$ -bonding) and  $\beta^2$  (covalent in-plane  $\pi$ -bonding). The in-plane  $\sigma$ -bonding parameter,  $\alpha^2$  is related to  $g_{\parallel}$  and  $g_{\perp}$  according to the following equation:

$$\alpha^2 = (A_{\parallel}/0.036) + (g_{\parallel} - 2.0027) + 3/7(g_{\perp} - 2.0027) + 0.04 \quad (4)$$

**Table 1**

The spin Hamiltonian parameters of copper complexes in DMSO solution at 300 and 77 K.

Complex	$A_{  }$	$A_{\perp}$	$A_{iso}$	$g_{  }$	$g_{\perp}$	$g_{iso}$	G	$g_{  }/A_{  }$	$\alpha^2$	$\beta^2$	$\gamma^2$	$K_{  }^2$	$K_{\perp}^2$
[Cu(L)(Gly) <sub>2</sub> ]	170	120	136	2.3336	2.0600	2.1512	5.8170	137	0.8669	0.6857	0.4715	0.5945	0.1021
[Cu(L)(Ala) <sub>2</sub> ]	150	110	123	2.3759	2.0795	2.1783	4.8847	158	0.8620	0.6688	0.5476	0.5765	0.1180
[Cu(L)(Val) <sub>2</sub> ]	171	94	120	2.3797	2.1665	2.2375	5.4938	132	0.7860	0.6184	0.0929	0.7017	0.3043

If  $\alpha^2 = 1.0$ , it indicates complete ionic character whereas  $\alpha^2 = 0.5$  denotes 100% covalent bonding, with assumption of negligible small values of the overlap integral. Here, in the present study the values of  $\alpha^2$  for the complexes [Cu(L)(Gly)<sub>2</sub>], [Cu(L)(Ala)<sub>2</sub>] and [Cu(L)(Val)<sub>2</sub>] are 0.8669, 0.8620 and 0.7860 respectively which indicate that metal–ligand bonds have some covalent character in-plane  $\sigma$  bonding. The out-plane  $\sigma$  bonding is not strong in the present study. This is due to demand of crystal packing forces on the interstitial site. The out-of-plane  $\pi$  bonding ( $\gamma^2$ ) and in-plane  $\pi$ -bonding ( $\beta^2$ ) parameters have been calculated from the following expressions:

$$\beta^2 = (g_{||} - 2.0027)E / -8\lambda\alpha^2 \quad (5)$$

$$\gamma^2 = (g_{\perp} - 2.0023)E / (-2\lambda\alpha^2) \quad (6)$$

where  $\lambda = -828 \text{ cm}^{-1}$  for free Cu(II) ion and  $E$  is the electronic transition energy of  ${}^2E_g \rightarrow {}^2T_{2g}$ . The observed values of  $\beta^2$  for the complexes [Cu(L)(Gly)<sub>2</sub>], [Cu(L)(Ala)<sub>2</sub>] and [Cu(L)(Val)<sub>2</sub>] are 0.6857, 0.6688 and 0.6184 and the values of  $\gamma^2$  are 0.475, 0.5476 and 0.0929 respectively. In this study,  $\beta^2 > \gamma^2$  which indicates that there is an interaction in out-of-plane  $\pi$ -bonding. Hathaway [30] pointed out that for pure  $\sigma$ -bonding,  $K_{||} \approx K_{\perp}$  and for in-plane  $\pi$ -bonding  $K_{||} < K_{\perp}$ , while for out-of-plane  $\pi$ -bonding  $K_{\perp} < K_{||}$  the following simplified expressions were used to calculate  $K_{||}$  and  $K_{\perp}$ :

$$K_{||} = (g_{||} - 2.0027)E / 8\lambda_0 \quad (7)$$

$$K_{\perp} = (g_{\perp} - 2.0027)E / 2\lambda_0 \quad (8)$$

The observed  $K_{||}$  for the complexes [Cu(L)(Gly)<sub>2</sub>], [Cu(L)(Ala)<sub>2</sub>] and [Cu(L)(Val)<sub>2</sub>] are 0.5945, 0.5765 and 0.7017 and  $K_{\perp}$  are 0.1021, 0.1180 and 0.3043 respectively which imply a greater contribution from out-of-plane  $\pi$ -bonding than from in-plane  $\pi$ -bonding in metal ligand  $\pi$ -bonding. Thus, the EPR study of the copper(II) complexes has provided supportive evidence to the conclusion obtained on the basis of electronic spectra and magnetic moment values.

### 3.6. DNA binding studies of metal complexes by optical method

One of the primary methods of observing and quantifying DNA is through the use of optics. Electronic absorption spectroscopy is universally employed to determine the binding characteristics of metal complex with DNA. Binding of the macromolecule leads to changes in the electronic spectrum of the metal complex. Base binding is expected to perturb the ligand field transition of the metal complex. A complex bound to DNA through intercalation is characterized by the change in absorbance (hypochromism) and red shift in wavelength, due to the intercalative mode involving a stacking interaction between the aromatic chromophore and the DNA base pairs. The extent of hypochromism is commonly consistent with the strength of the intercalative interaction [31]. On the other hand, metal complexes, which bind non-intercalatively or electrostatically with DNA may result in hyperchromism or hypochromism [32,33].

The binding mode of complexes to CT-DNA helix has been followed through absorption spectral titrations. With increasing

concentration of CT-DNA, the absorption bands of the complexes are affected, resulting in the tendency of hypochromism and a minor red shift is observed in all the complexes. With increasing DNA concentration, the absorption bands at 336.4, 281.0 and 260.9 nm for the complexes [Cu(L)(Gly)<sub>2</sub>], [Cu(L)(Ala)] and [Cu(L)(Val)<sub>2</sub>] are appeared with hypochromism of 11.3%, 11.61% and 18.24% respectively. The absorption bands at 339.8, 342.3 and 341.8 nm for cobalt complexes [Co(L)(Gly)<sub>2</sub>], [Co(L)(Ala)] and [Co(L)(Val)<sub>2</sub>] are appeared with hypochromism of 3.08%, 3.55% and 11.50% respectively. The absorption bands at 339.8, 340.2 and 330.2 nm for [Ni(L)(Gly)<sub>2</sub>], [Ni(L)(Ala)] and [Ni(L)(Val)<sub>2</sub>] complexes are appeared with hypochromism of 7.34%, 13.10% and 22.0% respectively. The absorption bands at 339.6, 339.6 and 339.0 nm for [Zn(L)(Gly)<sub>2</sub>], [Zn(L)(Ala)] and [Zn(L)(Val)<sub>2</sub>] complexes are appeared with hypochromism of 1.10%, 9.11% and 8.15% respectively. The electronic absorption spectra of most of the complexes in 5 mM Tris–HCl buffer (pH 7.2) are similar in shape and exhibit broad absorption bands in the range of 321.5–306.5 nm which are typical for transitions between the  $\pi$ -electronic energy levels (Figs. 1 and 2). It is also reported that the intense absorption bands (in the UV region) observed for the complexes are attributed to intraligand  $\pi$ – $\pi^*$  transition of the coordinated groups. On increasing the concentration of CT-DNA results in the minor bathochromic shift in the range  $\sim 0.2$ – $2.6$  nm and significant hypochromicity lying in the range  $\sim 3.08$ – $22.0\%$  which indicates that all the complexes are weak intercalator to the CT-DNA.

The intrinsic binding constants ( $K_b$ ) of the metal complexes with CT-DNA have been obtained by monitoring the changes in the intraligand band with increasing concentration of DNA. The  $K_b$  values are shown in Table 2, which shows the intrinsic binding constants for the complexes [Cu(L)(Gly)<sub>2</sub>], [Cu(L)(Ala)] and [Cu(L)(Val)<sub>2</sub>] are found to be  $5.559 \times 10^3$ ,  $8.613 \times 10^3$  and  $3.8271 \times 10^4 \text{ M}^{-1}$  respectively.

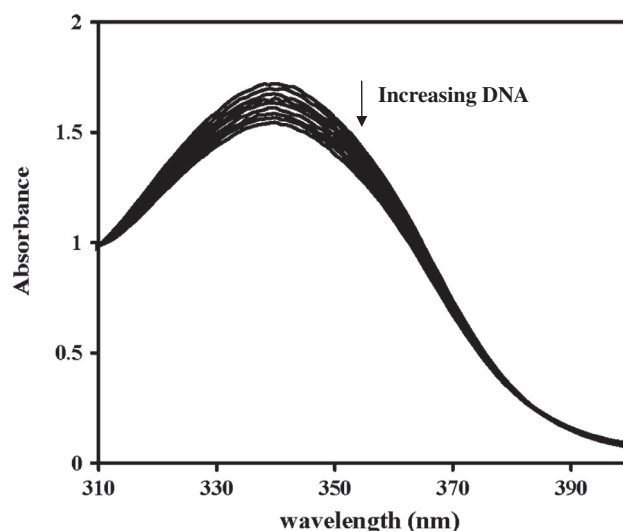


**Fig. 1.** Electronic absorption spectra of [Ni(L)(Ala)<sub>2</sub>] in the absence and presence of increasing amounts of DNA. {[Complex] = 10  $\mu\text{M}$ , [DNA] = 20–180  $\mu\text{M}$  from top to bottom}. Arrow indicates the change in the absorbance upon increasing the DNA concentration.

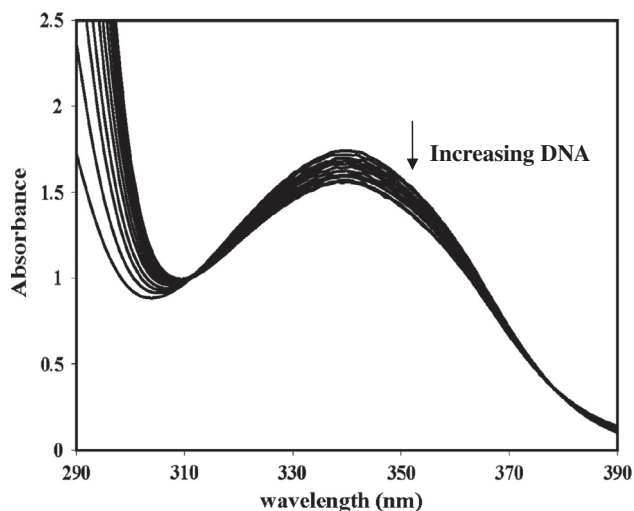


**Fig. 2.** Electronic absorption spectra of  $[\text{Ni}(\text{L})(\text{Val})_2]$  in the absence and presence of increasing amounts of DNA.  $[\text{Complex}] = 10 \mu\text{M}$ ,  $[\text{DNA}] = 20\text{--}180 \mu\text{M}$  from top to bottom). Arrow indicates the change in the absorbance upon increasing the DNA concentration.

The binding constants for  $[\text{Co}(\text{L})(\text{Gly})_2]$ ,  $[\text{Co}(\text{L})(\text{Ala})]$  and  $[\text{Co}(\text{L})(\text{Val})_2]$  complexes are  $1.034 \times 10^3$ ,  $2.766 \times 10^3$  and  $3.1055 \times 10^4 \text{ M}^{-1}$  respectively. For the nickel complexes the binding constant values are  $3.6955 \times 10^3$ ,  $4.4614 \times 10^4$  and  $3.8991 \times 10^5 \text{ M}^{-1}$  respectively. Finally for the zinc complexes the binding values are  $1.573 \times 10^3$ ,  $9.3590 \times 10^4$  and  $2.3355 \times 10^4 \text{ M}^{-1}$  respectively. The result suggests that the interaction of metal(II) complexes with DNA is significantly through weak intercalation mode. The binding constant ( $K_b$ ) values of these complexes are lower in comparison to those observed for typical intercalators, ethidium bromide and  $[\text{Ru}(\text{bpy})_2(\text{HBT})]^{2+}$  whose binding constants are in the order of  $7 \times 10^7$  and  $5.71 \times 10^7 \text{ M}^{-1}$  [34,35]. Based on the observed results, it is concluded that valine mixed ligand complexes are having higher binding constants than alanine and glycine mixed ligand complexes. Among the four complexes all nickel mixed ligand complexes are having higher binding constants than other complexes. Next higher binding constants have been observed in all copper mixed ligand complexes and the least binding values are found in the all zinc mixed ligand complexes. It can also be explained with the help of hypochromism which is directly related to the binding constant of the complexes. From this analysis (Table 2), it can be known that

**Table 2**  
Electronic absorption spectral properties of Cu(II), Co(II), Ni(II) and Zn(II) amino acid mixed ligand complexes.

No	Compound	$\lambda_{\text{max}}$		$\Delta\lambda$ (nm)	$^a\text{H\%}$	$^bK_b$ ( $\text{M}^{-1}$ )
		Free	Bound			
1	$[\text{Cu}(\text{L})(\text{Gly})_2]$	336.4	337.8	1.4	11.33	$5.559 \times 10^3$
2	$[\text{Co}(\text{L})(\text{Gly})_2]$	339.8	339.6	0.2	3.08	$1.034 \times 10^3$
3	$[\text{Ni}(\text{L})(\text{Gly})_2]$	339.8	339.4	0.4	7.34	$3.695 \times 10^3$
4	$[\text{Zn}(\text{L})(\text{Gly})_2]$	339.6	340.2	0.6	1.10	$1.573 \times 10^3$
5	$[\text{Cu}(\text{L})(\text{Ala})_2]$	281.0	280.6	0.4	11.61	$8.613 \times 10^3$
6	$[\text{Co}(\text{L})(\text{Ala})_2]$	342.3	341.0	1.3	3.55	$2.766 \times 10^3$
7	$[\text{Ni}(\text{L})(\text{Ala})_2]$	340.2	338.8	1.4	13.10	$4.4614 \times 10^4$
8	$[\text{Zn}(\text{L})(\text{Ala})_2]$	339.6	339.8	0.2	9.11	$9.3590 \times 10^3$
9	$[\text{Cu}(\text{L})(\text{Val})_2]$	260.9	261.7	0.8	18.24	$3.8271 \times 10^4$
10	$[\text{Co}(\text{L})(\text{Val})_2]$	341.8	339.2	2.6	11.50	$3.1055 \times 10^4$
11	$[\text{Ni}(\text{L})(\text{Val})_2]$	340.2	341.4	1.2	22.00	$3.8991 \times 10^5$
12	$[\text{Zn}(\text{L})(\text{Val})_2]$	339.0	339.8	0.8	8.15	$2.3355 \times 10^4$

<sup>a</sup>  $\text{H\%} = [A_{\text{free}} - A_{\text{bound}}]/A_{\text{free}} \times 100\%$ .

<sup>b</sup>  $K_b$  = Intrinsic DNA binding constant determined from the UV-Vis absorption spectral titration.

binding constant depends on the size of the alkyl group present in the mixed ligand of amino acid. As the size of the alkyl group increases, it makes more damage on the double helical structure of the DNA. Moreover, the enhanced binding constant for the valine mixed ligand complexes may be due to higher magnetic moments, electronic spectral vibrations, increased in hypochromism value, higher DNA cleavage ability and lower current density.

### 3.7. Viscosity measurements

The nature of binding of the metal complexes to the CT-DNA is further investigated by viscometric studies. The relative specific viscosity of DNA has been determined by varying the concentration of the added metal complexes. Measuring the viscosity of DNA is a classical technique used to analyze the DNA binding mode in solution. In the absence of crystallographic structural data, hydrodynamic methods that are sensitive to DNA length change are regarded as the least ambiguous and the most critical tests of binding in solution. A classical intercalation model results in the lengthening of the DNA helix as the base pairs are separated to accommodate the binding molecule, leading to an increase in the DNA viscosity. However, a partial or weak or non-classical intercalation of ligand may bend (or kink) DNA helix, resulting in the decrease of its effective length and concomitantly its viscosity [36]. The plot of  $(\eta/\eta_0)^{1/3}$  vs  $[\text{complex}]/[\text{DNA}] = R$ ,  $\eta$  and  $\eta_0$  are the relative viscosities of DNA in the presence and absence of compound, respectively, gives a measure of the viscosity changes. The effects of all the complexes on the viscosity of CT-DNA are shown in Fig. 3. As expected, the known DNA intercalator ethidium bromide increases the relative viscosity of DNA double helix resulting from intercalation. In contrast, weak intercalation can cause an increase in the effective length of DNA leading to a minor increase in the effective length of DNA solution [37]. All the complexes exhibit minor increase in the relative viscosity of CT-DNA compared to ethidium bromide suggesting primarily weak interaction nature of the complexes.

### 3.8. Electrochemical detection binding of metal complexes with DNA

Cyclic and differential pulse voltammetric techniques are extremely useful in probing the nature and mode of DNA binding of metal complexes. Typical cyclic voltammogram of complex,  $[\text{Cu}(\text{L})(\text{Val})_2]$  in the absence and in the presence of varying amount of [DNA] is shown in Fig. 4. The incremental addition of CT-DNA to the complex causes decrease of anodic and cathodic peak current of the complex. This result shows that complex stabilizes the duplex (GC pairs) by intercalating way. The incremental addition of CT-DNA to the complex causes shift in the potential of peak in

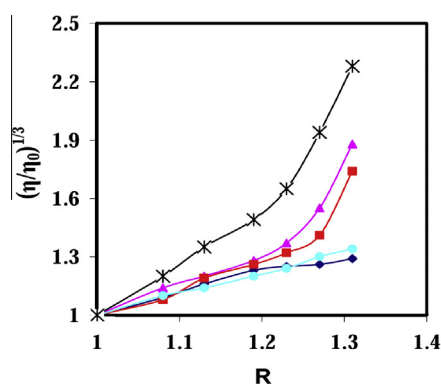


**Fig. 3.** Effect of increasing amounts of  $[\text{Ni}(\text{L})(\text{Val})_2]$  (▲),  $[\text{Cu}(\text{L})(\text{Val})_2]$  (■),  $[\text{Co}(\text{L})(\text{Val})_2]$  (●),  $[\text{Zn}(\text{L})(\text{Val})_2]$  (◆) and [EB] (\*) on the relative viscosity of CT-DNA.

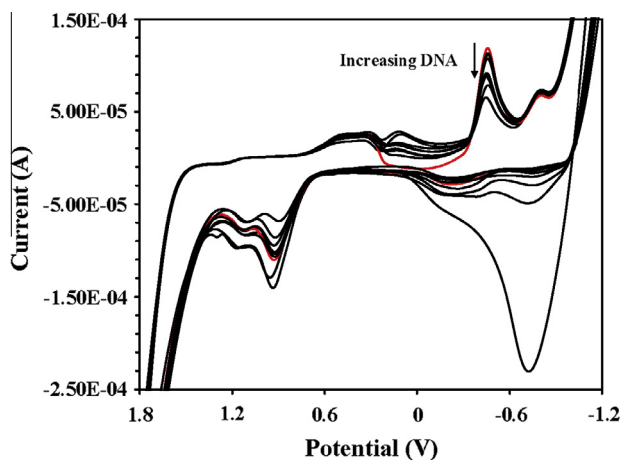


**Fig. 4.** Cyclic voltammogram of  $[\text{Cu}(\text{L})(\text{Val})_2]$  in the absence (—) and presence (—) of increasing amount of DNA concentration 10  $\mu\text{M}$ , 20  $\mu\text{M}$ , 40  $\mu\text{M}$ , 100  $\mu\text{M}$ , 150  $\mu\text{M}$ , 200  $\mu\text{M}$ , 250  $\mu\text{M}$ , respectively with scan rate of 10 mV/s. Supporting electrolyte, 5 mM Tris-HCl + 50 mM NaCl in water (pH 7.2).

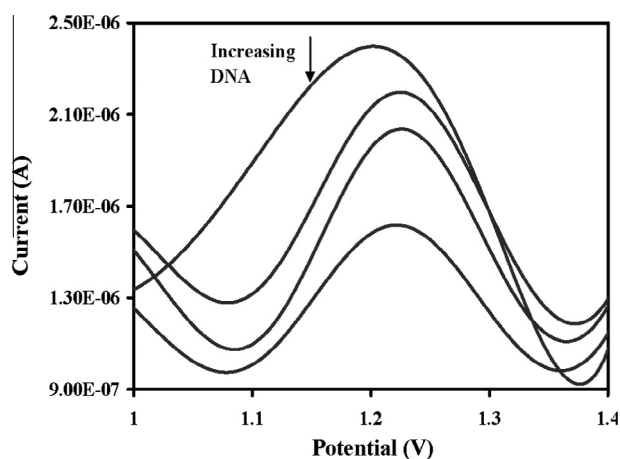


**Fig. 5.** Differential pulse voltammogram of 100  $\mu\text{M}$   $[\text{Co}(\text{L})(\text{Val})_2]$  complex in the absence and presence of DNA concentration 10  $\mu\text{M}$ , 20  $\mu\text{M}$ , 40  $\mu\text{M}$ , 100  $\mu\text{M}$ , 150  $\mu\text{M}$ , 200  $\mu\text{M}$ , 250  $\mu\text{M}$ , respectively with scan rate of 10 mV/s. Supporting electrolyte, 5 mM Tris-HCl + 50 mM NaCl in water (pH 7.2).

cyclic voltammogram. Both the cathodic and anodic peak show positive or negative shift which indicates intercalation of complex to DNA of base pairs. If one of the shifts is positive and another one is negative, it reveals the intercalation and electrostatic binding of the complex to CT-DNA or it may break the secondary structure of DNA.

In differential pulse voltammogram of the complex,  $[\text{Cu}(\text{L})(\text{Val})_2]$  in the absence and presence of varying amount of [DNA] with significant decrease of current intensity (Fig. 5), the shift in potential is related to the ratio of binding constant by the following equation:

$$E_b - E_f = 0.0591 \log(K_{[\text{red}]}/K_{[\text{oxd}]}) \quad (9)$$

where  $E_b$  and  $E_f$  are peak potentials of the complex in the bound and free form respectively. In the present study, **gly**, **ala** and **val** mixed ligand complexes show one electron transfer during the redox process and its  $I_{\text{pc}}/I_{\text{pa}}$  value is less than unity which indicates the reaction of the complex on the glassy carbon electrode surface is quasi-reversible. Other complexes  $[\text{Co}(\text{II})]$ ,  $[\text{Ni}(\text{II})]$  and  $[\text{Zn}(\text{II})]$  show considerable shift in both cathodic and anodic peak potentials in the presence of incremental addition of CT-DNA.

Most of the synthesized complexes give both the anodic and cathodic peak potential shifts which are either positive or negative. (Table 3). It indicates the intercalating mode of DNA binding with **gly/ala/val** mixed ligand Schiff base complexes. It is interesting to note that **val** mixed ligand complexes give greater decrease in current intensity than **ala/gly** mixed ligand complexes (Figs. 4 and 5). From this observation it is concluded that intercalative mode of DNA binding to val mixed ligand complexes is stronger than **ala/gly** mixed ligand complexes.

### 3.9. DNA cleavage studies

#### 3.9.1. DNA cleavage without adding reluctant

The ability of complex to cleave supercoiled DNA is determined by agarose gel electrophoresis. When circular plasmid DNA in the presence of an inorganic molecule is subjected to electrophoresis, relatively fast migration will be observed for the intact supercoiled form (Form I). If scission occurs on one strand, the super coil will relax to generate a slower moving open circular form (Form II). If both the strands are cleaved, a linear form (Form III) that migrates in between Form I and II will be generated [38]. The DNA cleavage ability of **gly**, **ala** and **val** mixed ligand complexes in DMF in the presence of Tris buffer medium is found out by Agarose gel electrophoresis pattern for the cleavage of pUC19 plasmid DNA.

**Table 3**

Electrochemical parameters for the interaction of DNA with metal(II) complexes of amino acid co-ligands.

S.No	Complexes	$^a E_{1/2}$ (V)		$^b \Delta E_{\text{p(V)}}$		$K_{\text{R}}/K_{\text{O}}$	$^c I_{\text{pc}}/I_{\text{pa}}$
		Free	Bound	Free	Bound		
1	$[\text{Cu}(\text{L})(\text{Gly})_2]$	-0.1235	-0.0985	+0.037	+0.065	0.8590	0.6782
2	$[\text{Co}(\text{L})(\text{Gly})_2]$	-0.1790	-0.1615	+0.036	+0.031	1.1640	0.6900
3	$[\text{Ni}(\text{L})(\text{Gly})_2]$	-0.6663	-0.6128	-0.0335	-0.0164	1.1294	0.5789
4	$[\text{Zn}(\text{L})(\text{Gly})_2]$	+0.1724	+0.1987	+0.0513	+0.0806	0.7421	0.7660
5	$[\text{Cu}(\text{L})(\text{Ala})_2]$	-0.139	-0.136	-0.0600	-0.0880	0.398	0.7312
6	$[\text{Co}(\text{L})(\text{Ala})_2]$	-0.2015	-0.2215	+0.0750	+0.0650	0.0341	0.6260
7	$[\text{Ni}(\text{L})(\text{Ala})_2]$	-0.1340	-0.1160	-0.0640	-0.0620	0.8590	0.8512
8	$[\text{Zn}(\text{L})(\text{Ala})_2]$	-0.4903	-0.4300	-0.0650	-0.0200	0.7357	1.0236
9	$[\text{Cu}(\text{L})(\text{Val})_2]$	-0.5267	-0.3882	-0.1298	-0.2185	1.2415	0.8419
10	$[\text{Co}(\text{L})(\text{Val})_2]$	-0.5045	-0.4800	+0.0630	+0.0220	2.1543	0.8240
11	$[\text{Ni}(\text{L})(\text{Val})_2]$	-0.1045	-0.0800	+0.0330	+0.0620	0.8264	0.9265
12	$[\text{Zn}(\text{L})(\text{Val})_2]$	-0.1657	-0.1637	+0.0728	+0.0242	0.6813	0.8740

Data from cyclic voltammetric measurements:

<sup>a</sup>  $E_{1/2}$  is calculated as the average of anodic ( $E_{\text{pa}}$ ) and cathodic ( $E_{\text{pc}}$ ) peak potentials.  $E_{1/2} = E_{\text{pa}} + E_{\text{pc}}/2$ .

<sup>b</sup>  $\Delta E_{\text{p}} = E_{\text{pa}} - E_{\text{pc}}$ .

<sup>c</sup> Error limit:  $\pm 5\%$ .

It has been observed that valine mixed ligand complexes have more DNA cleavage ability than alanine and glycine mixed ligand complexes. Among the valine mixed ligand complexes, nickel and copper complexes are having higher cleavage ability. These results are closely agreed with results of the binding studies. It is shown in Fig. 6. The DNA cleavage ability of  $[\text{Ni}(\text{L})(\text{Val})_2]$  complex has been investigated using pUC19 DNA in Tris buffer medium at 37 °C for 45 min. Control experiments suggest that untreated DNA does not show any cleavage upon irradiation, however with increasing concentration of  $[\text{Ni}(\text{L})(\text{Val})_2]$  complex, the amount of Form I of pUC19 DNA gradually diminishes, whereas that of Form II increases suggesting single strand DNA cleavage (Fig. 7).

### 3.9.2. In presence of activators

In order to probe the cleavage mechanism of pUC19 DNA induced by  $[\text{Ni}(\text{L})(\text{Val})_2]$  complex, the DNA cleavage activity has been evaluated in presence of different activators, viz. ascorbic acid (Asc),  $\text{H}_2\text{O}_2$ , 3-mercaptopropionic acid (MPA) and glutathione (GSH). As shown in Fig. 8 the nuclease activity of  $[\text{Ni}(\text{L})(\text{Val})_2]$  (30  $\mu\text{M}$ ) in DMF–Tris buffer medium in presence of activators follows the order  $\text{MPA} > \text{Asc} > \text{GSH} > \text{H}_2\text{O}_2$ .

### 3.9.3. In presence of radical scavengers

In order to clarify the cleavage mechanism of pUC19 DNA introduced by metal(II) complexes, the investigation is carried out further on adding DMSO, ethanol and t-BuOH (hydroxyl radical scavengers). It is found that there is no inhibition of DNA cleavage which indicates that hydroxyl radical is not involved in the cleavage process (Fig. 9, lanes 2–4). On the other hand, addition of L-histidine and sodium azide (singlet oxygen scavenger) does not show any apparent inhibition in the DNA which reveals that the singlet oxygen  $^1\text{O}_2$  is not responsible for the cleavage reaction (Fig. 9, lanes 5–7). These observations suggest that all the complexes mediated cleavage reaction have not proceeded via radical cleavage. SOD addition (Fig. 9, lanes 8 and 9) does not have any apparent effect on the cleavage activity indicating the non-involvement of super oxide radical in the cleavage reaction. Therefore, from these observations one can understand that the DNA cleavage proceeds via oxidative pathway.

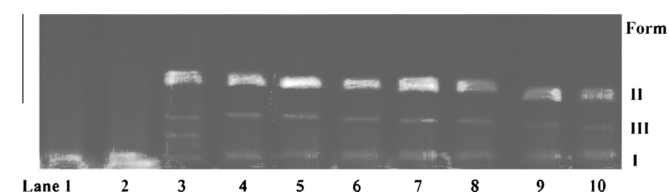


**Fig. 6.** Agarose gel electrophoresis pattern for the cleavage of pUC19 plasmid DNA (20  $\mu\text{M}$ ) with complex in DMF–Tris buffer medium; Lane 1: DNA control; Lane 2: Ligand 30  $\mu\text{M}$  complex + DNA; Lane 3:  $[\text{Ni}(\text{L})(\text{Val})_2]$  30  $\mu\text{M}$  complex + DNA; Lane 4:  $[\text{Cu}(\text{L})(\text{Val})_2]$  30  $\mu\text{M}$  complex + DNA; Lane 5:  $[\text{Co}(\text{L})(\text{Val})_2]$  30  $\mu\text{M}$  complex + DNA; Lane 6:  $[\text{Ni}(\text{L})(\text{Ala})_2]$  30  $\mu\text{M}$  complex + DNA; Lane 7:  $[\text{Cu}(\text{L})(\text{Ala})_2]$  30  $\mu\text{M}$  complex + DNA; Lane 8:  $[\text{Co}(\text{L})(\text{Ala})_2]$  30  $\mu\text{M}$  complex + DNA; Lane 9:  $[\text{Cu}(\text{L})(\text{Gly})_2]$  30  $\mu\text{M}$  complex + DNA; Lane 10:  $[\text{Ni}(\text{L})(\text{Gly})_2]$  30  $\mu\text{M}$  complex + DNA.

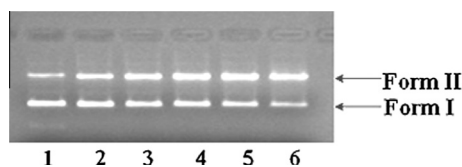


**Fig. 7.** Agarose gel electrophoresis pattern for the cleavage of pUC19 plasmid DNA (20  $\mu\text{M}$ ) with  $[\text{Ni}(\text{L})(\text{Val})_2]$  in DMF–Tris buffer medium; Lane 1: DNA control; Lane 2: 10  $\mu\text{M}$  complex + DNA; Lane 3: 15  $\mu\text{M}$  complex + DNA; Lane 4: 20  $\mu\text{M}$  complex + DNA; Lane 5: 25  $\mu\text{M}$  complex + DNA; Lane 6: 30  $\mu\text{M}$  complex + DNA.

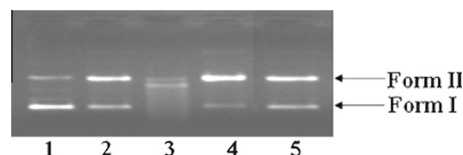


**Fig. 8.** Agarose gel electrophoresis pattern for the cleavage pattern of pUC19 plasmid DNA (20  $\mu\text{M}$ ) by  $[\text{Ni}(\text{L})(\text{Val})_2]$  (30  $\mu\text{M}$ ) in DMF–Tris buffer medium in presence of different activating agents at 37 °C after incubation for 30 min. Lane 1, DNA control; Lane 2, DNA + complex +  $\text{H}_2\text{O}_2$  (20  $\mu\text{M}$ ); Lane 3, DNA + complex + Asc (20  $\mu\text{M}$ ); Lane 4, DNA + complex + GSH (20  $\mu\text{M}$ ); Lane 5, DNA + complex + MPA (20  $\mu\text{M}$ ).

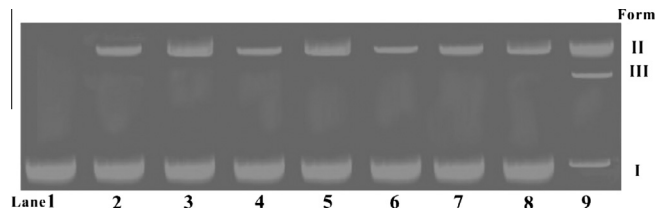


**Fig. 9.** Gel electrophoresis diagram showing the cleavage of supercoiled pUC19 DNA (20  $\mu\text{M}$ ) by  $[\text{Ni}(\text{L})(\text{Val})_2]$  (50  $\mu\text{M}$ ) with addition of MPA (100  $\mu\text{M}$ ) and radical scavengers in 5 Tris buffer medium and incubated at 37 °C for 1 h: Lane 1, DNA control; Lane 2, DNA +  $[\text{Ni}(\text{L})(\text{Val})_2]$  + DMSO (4  $\mu\text{L}$ ); Lane 3, DNA +  $[\text{Ni}(\text{L})(\text{Val})_2]$  + ethanol (4  $\mu\text{L}$ ); Lane 4, DNA +  $[\text{Ni}(\text{L})(\text{Val})_2]$  + t-BuOH (100  $\mu\text{M}$ ); Lane 5, DNA +  $[\text{Ni}(\text{L})(\text{Val})_2]$  + L-histidine (100  $\mu\text{M}$ ); Lane 6, DNA +  $[\text{Cu}(\text{L})(\text{Val})_2]$  +  $\text{NaN}_3$  (100  $\mu\text{M}$ ); Lane 7, DNA +  $[\text{Ni}(\text{L})(\text{Val})_2]$  +  $\text{NaN}_3$  (100  $\mu\text{M}$ ); Lane 8, DNA +  $[\text{Cu}(\text{L})(\text{Val})_2]$  + SOD (4 Units); Lane 9, DNA +  $[\text{Ni}(\text{L})(\text{Val})_2]$  + SOD (4 Units) respectively.

### 3.10. Antimicrobial screening

The main aim of the production and synthesis of any antimicrobial compound is to inhibit the causal microbe without any side effects on the patients. In addition, it is worthy to stress here on the basic idea of applying any chemotherapeutic agent which depends essentially on the specific control of only one biological function and not multiple ones. The chemotherapeutic agent affecting only one function has a highly sounding application in the field of treatment by anticancer, since most of the anticancer used in the present time affect both cancerous diseased cells and healthy ones which in turns affect the general health of the patients. Therefore, there is a real need for having a chemotherapeutic agent which controls only one function. Introducing metal ions into a biological system may be carried out for therapeutic and diagnostic purpose.

To support in the field of bioinorganic chemistry, subsequently, the compounds synthesized have been evaluated for their antibacterial and antifungal actions. The antibacterial and antifungal tests have been carried out using the disc diffusion method. The organisms used in present investigation include the bacteria *Staphylococcus aureus*, *Pseudomonas aeruginosa*, *Escherichia coli*, *Staphylococcus epidermidis*, *Klebsiella pneumoniae* and the fungal species *Aspergillus niger*, *Aspergillus flavus*, *Culvularia lunata*, *Rhizocotonia bataicola* and *Candida albicans*. The effectiveness of the investigated ligand and its metal complexes as good antimicrobial agents has been screened in addition to evaluation of few known antibiotics using streptomycin as standard antibacterial agent and nystatin as antifungal agent. The results of the antimicrobial studies of the synthesized compounds are displayed in Table 4 and Table 5. All the complexes are more potent than the ligand towards the specified bacterial and fungal species. Moreover, all the complexes are having antimicrobial activities that are very close to the standard streptomycin and nystatin. Most of the complexes are having better activities towards *P. aeruginosa*, *E. coli*, *S. epidermidis* and fungal species.

**Table 4**The *in vitro* antibacterial activity of ligand and its amino acid mixed ligand complexes evaluated by MIC (Minimum Inhibitory Concentration, µg/mL).

Compound	<i>S. aureus</i>	<i>P. aeruginosa</i>	<i>E. coli</i>	<i>S. epidermidis</i>	<i>K. pneumoniae</i>
FFAP (L)	23.8 ± 0.12	8.9 ± 0.61	20.3 ± 0.65	21.7 ± 0.23	24.4 ± 0.45
[Cu(L)(Gly) <sub>2</sub> ]	6.0 ± 0.82	4.5 ± 0.24	3.6 ± 0.18	6.0 ± 0.46	4.8 ± 0.15
[Co(L)(Gly) <sub>2</sub> ]	7.2 ± 1.02	6.3 ± 0.86	2.1 ± 0.78	1.4 ± 1.03	13.5 ± 0.69
[Ni(L)(Gly) <sub>2</sub> ]	5.7 ± 0.23	1.6 ± 0.19	1.8 ± 0.42	6.3 ± 0.39	6.0 ± 0.47
[Zn(L)(Gly) <sub>2</sub> ]	4.8 ± 1.12	1.8 ± 0.88	1.9 ± 1.16	4.2 ± 0.68	2.9 ± 1.03
[Cu(L)(Ala) <sub>2</sub> ]	7.2 ± 0.23	2.4 ± 0.42	1.6 ± 0.25	1.8 ± 0.44	6.36 ± 0.36
[Co(L)(Ala) <sub>2</sub> ]	5.4 ± 0.38	2.1 ± 0.75	1.9 ± 0.14	1.3 ± 0.52	4.8 ± 0.73
[Ni(L)(Ala) <sub>2</sub> ]	5.4 ± 0.51	2.3 ± 0.28	3.0 ± 0.49	3.0 ± 0.58	6.6 ± 0.14
[Zn(L)(Ala) <sub>2</sub> ]	7.2 ± 1.18	3.0 ± 1.06	1.8 ± 0.40	3.0 ± 1.08	7.8 ± 0.87
[Cu(L)(Val) <sub>2</sub> ]	12.3 ± 0.16	1.8 ± 0.24	1.5 ± 0.18	1.8 ± 0.11	11.2 ± 0.14
[Co(L)(Val) <sub>2</sub> ]	13.4 ± 1.02	2.6 ± 1.15	2.4 ± 0.28	1.2 ± 0.64	12.3 ± 0.18
[Ni(L)(Val) <sub>2</sub> ]	12.3 ± 0.25	2.1 ± 0.17	1.9 ± 0.13	1.2 ± 0.25	10.5 ± 0.44
[Zn(L)(Val) <sub>2</sub> ]	13.5 ± 0.96	1.6 ± 0.92	1.5 ± 0.48	2.4 ± 0.68	13.4 ± 0.28
DMSO	–	–	–	–	–
Streptomycin <sup>a</sup>	1.7 ± 0.08	1.9 ± 0.11	1.8 ± 0.05	1.3 ± 0.14	2.3 ± 0.18

<sup>a</sup> Streptomycin is used as a standard drug; Error limit: ±2%.**Table 5**The *in vitro* antifungal activity of ligand and its amino acid mixed ligand complexes evaluated by MIC (Minimum Inhibitory Concentration, µg/mL).

Compound	<i>A. niger</i>	<i>A. flavus</i>	<i>C. lunata</i>	<i>R. bataticola</i>	<i>C. albicans</i>
FFAP (L)	25.3 ± 1.02	8.4 ± 0.98	18.3 ± 0.86	21.7 ± 1.13	26.4 ± 1.26
[Cu(L)(Gly) <sub>2</sub> ]	7.0 ± 0.23	6.0 ± 0.26	4.1 ± 0.32	8.0 ± 0.41	5.8 ± 0.52
[Co(L)(Gly) <sub>2</sub> ]	9.2 ± 0.28	7.8 ± 0.36	2.6 ± 0.43	3.4 ± 0.51	14.5 ± 0.68
[Ni(L)(Gly) <sub>2</sub> ]	6.7 ± 0.85	3.1 ± 0.49	2.3 ± 0.58	8.3 ± 0.62	7.0 ± 0.87
[Zn(L)(Gly) <sub>2</sub> ]	5.8 ± 1.12	3.3 ± 0.92	2.4 ± 0.86	6.2 ± 0.78	3.9 ± 0.82
[Cu(L)(Ala) <sub>2</sub> ]	9.2 ± 0.11	3.9 ± 0.15	2.2 ± 0.23	3.8 ± 0.28	7.3 ± 0.31
[Co(L)(Ala) <sub>2</sub> ]	7.4 ± 0.13	3.6 ± 0.22	2.6 ± 0.30	3.3 ± 0.36	5.8 ± 0.38
[Ni(L)(Ala) <sub>2</sub> ]	7.1 ± 0.68	3.8 ± 0.95	3.7 ± 0.15	5.0 ± 0.46	7.6 ± 0.52
[Zn(L)(Ala) <sub>2</sub> ]	10.2 ± 0.28	4.5 ± 0.85	2.5 ± 0.57	5.2 ± 0.63	8.8 ± 0.88
[Cu(L)(Val) <sub>2</sub> ]	15.3 ± 0.06	4.2 ± 0.10	3.1 ± 0.15	3.0 ± 0.09	12.2 ± 0.12
[Co(L)(Val) <sub>2</sub> ]	17.4 ± 0.08	3.6 ± 0.13	3.0 ± 0.21	3.2 ± 0.15	13.3 ± 0.18
[Ni(L)(Val) <sub>2</sub> ]	14.3 ± 0.86	3.6 ± 0.58	1.8 ± 0.17	3.2 ± 0.59	11.5 ± 0.65
[Zn(L)(Val) <sub>2</sub> ]	15.5 ± 1.06	3.1 ± 0.69	2.1 ± 0.87	5.4 ± 0.53	14.3 ± 0.41
DMSO	–	–	–	–	–
Nystatin <sup>a</sup>	1.1 ± 0.12	1.7 ± 0.09	1.2 ± 0.25	1.0 ± 0.04	1.5 ± 0.16

<sup>a</sup> Nystatin is used as a standard drug; Error limit: ±2%.

The results obtained show that the mixed ligand complexes are more toxic than the ligand against the same microorganisms. This enhancement in the activity is rationalized on the basis of the structure of the metal complexes by possessing an additional azomethine (HC=N) linkage which imports in elucidating the mechanism of transamination and resamination reactions in biological system. It has been suggested that the ligands with nitrogen and oxygen donor systems might restrain enzyme production, since the enzymes which require these group for their activity appear to be especially more susceptible to deactivation by the metal ions upon chelation. All the complexes are more active against more organisms comparable to the Schiff base ligand. The rise in the antimicrobial activity of the mixed ligand complexes may be owing to the effect of the metal ion on the normal cell processes. This is probable due to the greater lipophilic nature of the complexes. Such increased activity of the metal chelates can be explained on the basis of chelation theory. While chelation is not the only criterion for antibacterial activity, it is an intricate blend of several factors such as the nature of the metal ion and the ligand, the geometry of the metal complexes, the lipophilicity and the presence of co-ligands, the steric and pharmacokinetic factors.

### 3.11. Antioxidant potency

According to relevant reports in the literature [39–42], few transition metal complexes may exhibit antioxidant activity. It is

therefore also conducted an investigation to explore whether the synthesized complex has the hydroxyl radical scavenging property. The ability of one of the present compounds is compared to scavenge hydroxyl radicals with those of the well-known natural antioxidants mannitol and vitamin C, using the same method as reported by Wu et al. [43]. The 50% inhibitory concentration (IC<sub>50</sub>) values of mannitol and vitamin C are about  $9.6 \times 10^{-3}$  and  $8.7 \times 10^{-3} \text{ M}^{-1}$ , respectively. According to the antioxidant experiments, the IC<sub>50</sub> values of [Ni(L)(Gly)<sub>2</sub>] and [Cu(L)(Gly)<sub>2</sub>] complexes are  $2.12 \times 10^{-8} \text{ M}^{-1}$  and  $1 \times 10^{-6} \text{ M}^{-1}$  respectively which imply that [Ni(L)(Gly)<sub>2</sub>] complex has preferable ability to scavenge hydroxyl radical. In view of the observed IC<sub>50</sub> values, the [Ni(L)(Gly)<sub>2</sub>] complex can be considered as a potential drug to eliminate the hydroxyl radical. The antioxidant behaviour is also observed in all alanine mixed ligand complexes. The IC<sub>50</sub> values of [Cu(L)(Ala)<sub>2</sub>], [Co(L)(Ala)<sub>2</sub>], [Ni(L)(Ala)<sub>2</sub>] and [Zn(L)(Ala)<sub>2</sub>] complexes are  $1 \times 10^{-6}$ ,  $1 \times 10^{-7}$ ,  $1 \times 10^{-5}$  and  $1 \times 10^{-7} \text{ M}^{-1}$  respectively. These values show that Co(II), Zn(II), Cu(II) and Ni(II) alanine mixed ligand complexes have preferable ability to scavenge hydroxyl radical. On comparing those IC<sub>50</sub> values, it can be shown that [Ni(L)(Gly)<sub>2</sub>], [Co(L)(Ala)<sub>2</sub>], [Zn(L)(Ala)<sub>2</sub>], [Cu(L)(Ala)<sub>2</sub>] and [Ni(L)(Ala)<sub>2</sub>] complexes can be considered as potential drugs to eliminate the hydroxyl radical.

## 4. Conclusion

Novel mononuclear 4-aminoantipyrine derived Schiff base ligand and amino acid mixed ligand Cu(II), Ni(II), Co(II), and Zn(II) complexes have been characterized by spectral and analytical data. The IR, electronic transition and g tensor data lead to the conclusion that the Cu(II) ion assumes a distorted octahedral geometry and the other complexes Ni(II), Co(II) and Zn(II) are octahedral in nature. In all the complexes, the Schiff base ligand acts as a bidentate. DNA-binding properties of synthetic metal complexes have been comprehensively studied by different methods including electronic absorption spectra, viscosity measurements, cyclic voltammetry analysis. All results suggest that the complexes interact with DNA through a weak intercalation binding mode. In addition, the DNA cleavage ability of glycine, alanine and valine mixed ligand complexes in DMF in presence of Tris buffer medium is found out by Agarose gel electrophoresis pattern for the cleavage of pUC19 plasmid DNA. It has been observed that valine mixed ligand complexes have more DNA cleavage ability than alanine and glycine mixed ligand complexes. Among the valine mixed ligand complexes, nickel and copper complexes are having higher cleavage ability. These results are closely agreed with the results of the

binding studies. The cleavage studies suggest that all the complexes mediated cleavage reaction have not proceed via radical cleavage. Antimicrobial activity studies show that the complexes exhibit good biological activity against different organisms as compared to ligand and standards. These studies assume significance as they provide the comprehension of binding of transition metal complexes to DNA and for developing the next generation of DNA binding and anticancer drugs.

### Acknowledgements

The authors express their sincere thanks to the College Managing Board, Principal and Head of the Department of Chemistry, VHNSN College for providing necessary research facilities. They also thank the Sophisticated Analytical and Instrumentation Facility, Central Drug Research Institute, Lucknow, for providing CHN-analysis data and FAB-Mass spectra and Sophisticated Analytical and Instrumentation Facility, Indian Institute of Technology, Bombay, for EPR measurements.

### Appendix A. Supplementary material

Supplementary data associated with this article can be found, in the online version, at <http://dx.doi.org/10.1016/j.molstruc.2013.12.018>.

### References

- [1] H.K. Liu, P.J. Sadler, *Acc. Chem. Res.* 44 (2011) 349–359.
- [2] U. Jungwirth, C.R. Kowol, B.K. Keppler, C.G. Hartinger, W. Berger, P. Heffeter, *Antioxid. Redox Signal.* 15 (2011) 1085–1127.
- [3] S.L.H. Higgins, T.A. White, B.S.J. Winkel, K.J. Brewer, *Inorg. Chem.* 50 (2011) 463–470.
- [4] M. Cusumano, M.L. Di Pietro, A. Giannetto, *Inorg. Chem.* 45 (2006) 230–235.
- [5] K. Abdi, H. Hadadzadeh, M. Weil, M. Salimi, *Polyhedron* 31 (2012) 638–648.
- [6] C. Li, S.L. Liu, L.H. Guo, D.P. Chen, *Electrochem. Commun.* 7 (2005) 23–28.
- [7] L.H. Hurley, *Nat. Rev.* 2 (2002) 188–200.
- [8] S. Tabassum, M. Zaki, M. Afzal, F. Arjmand, *Dalton Trans.* 42 (2013) 10029–10041.
- [9] Z.D. Matovic, E. Mrkalic, G. Bogdanovic, V. Kojic, A. Meetsma, R. Jelic, *J. Inorg. Biochem.* 121 (2013) 134–144.
- [10] S. Ambika, S. Arunachalam, R. Arun, K. Premkumar, *RSC Adv.* 3 (2013) 16456–16468.
- [11] D. Dreher, A.F. Junod, *J. Cancer* 32 (1996) 30–38.
- [12] W.J. Chen, P. Guo, J. Song, W. Cao, J. Bian, *Bioorg. Med. Chem. Lett.* 16 (2006) 3582–3585.
- [13] J.R.J. Sorenson, *Chem. Br.* 20 (1984) 1110–1113.
- [14] N. Raman, S. Sobha, *Spectrochim. Acta* 85A (2012) 223–229.
- [15] P. Kumar, A.K. Singh, J.K. Saxena, D.S. Pandey, *J. Organomet. Chem.* 694 (2009) 3570.
- [16] C.M. Metcalfe, S. Spey, H. Adams, J.A.J. Thomas, *Chem. Soc. Dalton Trans.* (2002) 4732–4739.
- [17] A. Amboise, B.J. Maiya, *Inorg. Chem.* 39 (2000) 4256–4263.
- [18] J. Marmur, *J. Mol. Biol.* 3 (1961) 208–218.
- [19] J.B. Charies, N. Dattagupta, D.M. Crothers, *Biochemistry* 21 (1982) 3933–3940.
- [20] S. Satyanarayanan, J.C. Davorusak, J.B. Charies, *Biochemistry* 32 (1993) 2573–2584.
- [21] J.G. Cappuccino, N. Sherman, *Microbiology Lab Manual*, fourth ed., Benjamin/Cummings Publishing Company, Inc, 1996.
- [22] C.C. Winterbourn, *Biochem. J.* 198 (1981) 125–131.
- [23] C.C. Winterbourn, *Biochem. J.* 182 (1979) 625–628.
- [24] Z. Guo, R. Xing, S. Liu, H. Yu, P. Wang, C. Li, P. Li, *Bioorg. Med. Chem. Lett.* 15 (2005) 4600–4603.
- [25] T.R. Holman, M.P. Hendrich, L. Que, *Inorg. Chem.* 31 (1992) 937–939.
- [26] J. Manonmani, M. Kandaswamy, V. Narayanan, R. Thirumurugan, S. Shanmuga Sundura Raj, G. Shanmugam, M.N. Ponnuswamy, H.K. Fun, *Polyhedron* 20 (2001) 3039–3048.
- [27] K. Karaoglu, T. Baran, K. Serbest, M. Er, I. Degirmencioglu, *J. Mol. Struct.* 922 (2009) 39–45.
- [28] N. Raman, S. Thalamuthu, J. Dhavethuraja, M.A. Neelakandan, S.J. Banerjee, *J. Chil. Chem. Soc.* 53 (2008) 1439–1443.
- [29] R.K. Ray, G.B. Kauffman, *Inorg. Chim. Acta* 173 (1990) 207–214.
- [30] B.J. Hathaway, *Structure and Bonding*, vol. 14, Springer Verlag, Heidelberg, 1973, p. 60.
- [31] C.N. Sudhamani, H.S. Bhojya Naik, T.R. Ravikumar Naik, M.C. Prabhakara, *Spectrochim. Acta* 72A (2009) 643–647.
- [32] D. Lawrence, V.G. Vaidyanathan, B. Unni Nair, *J. Inorg. Biochem.* 100 (2006) 1244–1251.
- [33] Q.S. Li, P. Yang, H.F. Wang, M.L. Guo, *J. Inorg. Biochem.* 64 (1996) 181–195.
- [34] M.J. Waring, *J. Mol. Biol.* 13 (1965) 269–282.
- [35] D.L. Arockiasamy, S. Radhika, R. Parthasarathi, B.U. Nair, *Eur. J. Med. Chem.* 44 (2009) 2044–2051.
- [36] S. Sathyanarayana, J.C. Dabrowiak, J.B. Chaires, *Biochemistry* 32 (1993) 2573–2584.
- [37] C. Rajput, R. Rutkaite, L. Swanson, I. Haq, J.A. Thomas, *Chemistry* 12 (2006) 4611–4619.
- [38] D.D. Li, J.L. Tian, W. Gu, X. Liu, H.H. Zeng, S.P. Yan, *J. Inorg. Biochem.* 105 (2011) 894–901.
- [39] S.B. Bukhari, S. Memon, M. Mahroof-Tahir, M.I. Bhangar, *Spectrochim. Acta* 71A (2009) 1901–1906.
- [40] F.V. Botelho, J.J. Alvarez-Leite, V.S. Lemos, A.M.C. Pimenta, H.D.R. Calado, T. Matencio, C.T. Miranda, E.C. Pereira-Maia, *J. Inorg. Biochem.* 101 (2007) 935–943.
- [41] Q. Wang, Z.Y. Yang, G.F. Qi, D.D. Qin, *Eur. J. Med. Chem.* 44 (2009) 2425–2433.
- [42] T.R. Li, Z.Y. Yang, B.D. Wang, D.D. Qin, *Eur. J. Med. Chem.* 43 (2008) 1688–1695.
- [43] H. Wu, J. Yuan, Y. Bai, G. Pan, H.W.X. Shu, *J. Photochem. Photobiol. B: Biol.* 107 (2012) 65–72.